

Parameterizations of US wildfire and prescribed fire emission ratios and emission factors based on FIREX-AQ aircraft measurements

Georgios I. Gkatzelis^{1,2,†}, Matthew M. Coggon², Chelsea E. Stockwell^{1,2}, Rebecca S. Hornbrook³, Hannah Allen⁴, Eric C. Apel³, Megan M. Bela^{1,2,Δ}, Donald R. Blake⁵, Ilann Bourgeois^{1,2,Ξ}, Steven S. Brown^{2,6}, Pedro Campuzano-Jost^{1,6}, Jason M. St. Clair^{7,8}, James H. Crawford⁹, John D. Crouse¹⁰, Douglas A. Day^{1,6}, Joshua P. DiGangi⁹, Glenn S. Diskin⁹, Alan Fried¹¹, Jessica B. Gilman², Hongyu Guo^{1,6}, Johnathan W. Hair⁹, Hannah S. Halliday^{9,‡}, Thomas F. Hanisco⁷, Reem Hannun^{7,12,⊖}, Alan Hills³, L. Gregory Huey¹³, Jose L. Jimenez^{1,6}, Joseph M. Katich^{1,2}, Aaron Lamplugh^{1,2}, Young Ro Lee¹³, Jin Liao^{7,14}, Jakob Lindaas^{15,§}, Stuart A. McKeen^{1,2}, Tomas Mikoviny¹⁶, Benjamin A. Nault^{1,6,||,⊖}, J. Andrew Neuman^{1,2}, John B. Nowak⁹, Demetrios Pagonis^{1,6,¶}, Jeff Peischl^{1,2}, Anne E. Perring^{1,17}, Felix Piel^{16,18,19}, Pamela S. Rickly^{1,2}, Michael A. Robinson^{1,2,6}, Andrew W. Rollins², Thomas B. Ryerson^{2,^}, Melinda K. Schueneman^{1,6}, Rebecca H. Schwantes², Joshua P. Schwarz², Kanako Sekimoto²⁰, Vanessa Selimovic²¹, Taylor Shingler⁹, David J. Tanner¹³, Laura Tomsche^{9,22,*,#}, Krystal T. Vasquez¹⁰, Patrick R. Veres^{2,9}, Rebecca Washenfelder², Petter Weibring¹⁰, Paul O. Wennberg^{10,23}, Armin Wisthaler^{16,18}, Glenn M. Wolfe⁷, Caroline C. Womack^{1,2}, Lu Xu^{10,+,&}, Katherine Ball⁴, Robert J. Yokelson²¹, Carsten Warneke²

Deleted: ²

¹ Cooperative Institute for Research in Environmental Sciences, University of Colorado Boulder, Boulder, CO, USA

² NOAA Chemical Sciences Laboratory (CSL), Boulder, CO, USA

³ Atmospheric Chemistry Observations & Modeling Laboratory, NCAR, Boulder, CO, USA

⁴ Division of Chemistry and Chemical Engineering, California Institute of Technology, Pasadena, CA, USA

⁵ Department of Chemistry, University of California, Irvine, CA, USA

⁶ Department of Chemistry, University of Colorado Boulder, Boulder, CO, USA

⁷ Atmospheric Chemistry and Dynamics Laboratory, NASA Goddard Space Flight Center, Greenbelt, MD, USA

⁸ Joint Center for Earth Systems Technology, University of Maryland Baltimore County, Baltimore, MD, USA

⁹ NASA Langley Research Center, Hampton, VA, USA

¹⁰ [Institute of Arctic and Alpine Research, University of Colorado, Boulder, CO, USA](#)

¹¹ Institute of Arctic & Alpine Research, University of Colorado, Boulder, CO, USA

¹² Joint Center for Earth Systems Technology, University of Maryland Baltimore County, Baltimore, MD, USA

¹³ School of Earth and Atmospheric Sciences, Georgia Institute of Technology, Atlanta, GA, USA

¹⁴ [Goddard Earth Sciences Technology and Research \(GESTAR II\), University of Maryland, Baltimore County, MD, USA](#)

¹⁵ Colorado State University, Department of Atmospheric Science, Fort Collins, CO, USA

¹⁶ Department of Chemistry, University of Oslo, Oslo, Norway

¹⁷ Department of Chemistry, Colgate University, Hamilton, NY, USA

¹⁸ Institut für Ionenphysik und Angewandte Physik, Universität Innsbruck, Innsbruck, Austria

¹⁹ IONICON Analytik GmbH, Innsbruck, Austria

²⁰ Graduate School of Nanobioscience, Yokohama City University, 22-2 Seto, Kanazawa-ku, Yokohama, Kanagawa, Japan

²¹ Department of Chemistry and Biochemistry, University of Montana, Missoula, MT, USA

²² Universities Space Research Association, Columbia, MD, USA

²³ Division of Engineering and Applied Science, California Institute of Technology, Pasadena, CA, USA

Currently at:

[†] Institute of Energy and Climate Research, IEK-8: Troposphere, Forschungszentrum Jülich GmbH, Jülich, Germany

[‡] U.S. Environmental Protection Agency, Research Triangle Park, NC, USA

^Δ [Department of Geology and Environmental Science, University of Pittsburgh, PA, USA](#)

[⊖] [Google](#)

[⊖] [Univ. Savoie Mont Blanc, INRAE, CARRTEL, Thonon-les-Bains, France](#)

[§] AGI / AAAS Congressional Science Fellow

Deleted: Division of Geological and Planetary Sciences, California Institute of Technology, Pasadena, CA, USA

Deleted: Universities Space Research Association, Columbia, MD, USA...

Deleted: ²⁴ Division of Chemistry and Chemical Engineering, California Institute of Technology, Pasadena, CA, USA

61 || Center for Aerosol and Cloud Chemistry, Aerodyne Research Inc., Billerica, MA, USA
62 || [Department of Environmental Health and Engineering, Johns Hopkins University, MD, USA](#)
63 || [¶] Weber State University, Ogden, UT, USA
64 || [^] Scientific Aviation, Boulder, CO, USA
65 || ^{*} Institute of Atmospheric Physics, German Aerospace Center, Wessling, Germany
66 || [#] Johannes Gutenberg University, Mainz, Germany
67 || ⁺ Cooperative Institute for Research in Environmental Sciences, University of Colorado Boulder, Boulder, CO,
68 || USA and NOAA Chemical Sciences Laboratory (CSL), Boulder, CO, USA
69 || [◇] [Earth Observing Laboratory, NCAR, Boulder, CO, USA](#)
70 || [×] [McKelvey School of Engineering, Washington University, MO, USA](#)

71 Correspondence to: (g.gkatzelis@juelich.de and matthew.m.coggon@noaa.gov)

72 **Abstract.**

73 Extensive airborne measurements of non-methane organic gases (NMOGs), methane, nitrogen oxides, reduced
74 nitrogen-species, and aerosol emissions from US wild and prescribed fires were conducted during the 2019
75 NOAA/NASA Fire Influence on Regional to Global Environments and Air Quality campaign (FIREX-AQ). Here,
76 we report the atmospheric enhancement ratios (ERs) and inferred emission factors (EFs) for compounds measured
77 onboard the NASA DC-8 research aircraft for nine wildfires and one prescribed fire, which encompass a range of
78 vegetation types.

79 We use photochemical proxies to identify young smoke and reduce the effects of chemical degradation on our
80 emissions calculations. ERs and EFs calculated from FIREX-AQ observations agree within a factor of 2 with values
81 reported from previous laboratory and field studies for more than 80% of the carbon- and nitrogen-containing
82 species. Wildfire emissions are parameterized based on correlations of the sum of NMOGs with reactive nitrogen
83 oxides (NO_y) to modified combustion efficiency (MCE) as well as other chemical signatures indicative of
84 flaming/smoldering combustion, including carbon monoxide (CO), nitrogen dioxide (NO₂), and black carbon
85 aerosol. The sum of primary NMOG EFs correlates to MCE with an R² of 0.68 and a slope of $-296 \pm 51 \text{ g kg}^{-1}$,
86 consistent with previous studies. The sum of the NMOG mixing ratios correlates well with CO with an R² of 0.98
87 and a slope of $137 \pm 4 \text{ ppbv}$ of NMOGs per ppmv of CO, demonstrating that primary NMOG emissions can be
88 estimated from CO. Individual nitrogen-containing species correlate better with NO₂, NO_y, and black carbon than
89 with CO. More than half of the NO_y in fresh plumes is NO₂ with an R² of 0.95 and a ratio of NO₂ to NO_y of $0.55 \pm$
90 $0.05 \text{ ppbv ppbv}^{-1}$, highlighting that fast photochemistry had already occurred in the sampled fire plumes. The ratio
91 of NO_y to the sum of NMOGs follows trends observed in laboratory experiments and increases exponentially with
92 MCE, due to increased emission of key nitrogen species and reduced emission of NMOGs at higher MCE during
93 flaming combustion. These parameterizations will provide more accurate boundary conditions for modeling and
94 satellite studies of fire plume chemistry and evolution to predict the downwind formation of secondary pollutants,
95 including ozone and secondary organic aerosol.

96 **1 Introduction**

97 Open biomass burning in the form of wildfires, prescribed forest management fires, and agricultural burns is one of
98 the largest sources of trace gases and aerosols worldwide (Akagi et al., 2011; Crutzen and Andreae, 1990). It is the
99 dominant global source of black carbon and primary organic aerosol (Bond et al., 2013), and accounts for more than
100 20% of the global emissions of nitric oxide (NO) and carbon monoxide (CO) (Olivier et al., 2005; Yokelson et al.,
101 2008; Wiedinmyer et al., 2011). It is the second largest global source of non-methane organic gases (NMOGs)
102 (Akagi et al., 2011), and a major source of greenhouse gases, including methane (CH₄), carbon dioxide (CO₂), and
103 nitrous oxide (N₂O) that impact the atmospheric carbon budget and climate (Sudo and Akimoto, 2007; Ward et al.,
104 2012; Tian et al., 2016; Le Quéré et al., 2018).

105 During the last decade, the number of wildfires and prescribed fires in the US has sometimes exceeded 74,000 and
106 450,000 yr⁻¹, respectively (National Interagency Fire Center). Warming temperatures, drier climate, and a history of
107 fire suppression are projected to increase the frequency and intensity of wildfires and lengthen fire seasons globally
108 (Spracklen et al., 2009; Kloster et al., 2010; Pechony and Shindell, 2010; Moritz et al., 2012; Flannigan et al., 2013;
109 Mann et al., 2016; Balch et al., 2017), which is already evident in the western US, Canada, the eastern Mediterranean,
110 Siberia, and Australia (Westerling et al., 2006; Keywood et al., 2013; Yue et al., 2015). Wildfires in the US largely
111 occur in the western conterminous states and Alaska, and typically account for 12 to 40 thousand km² of the annual
112 total area burned (National Interagency Fire Center). In the southeastern US, prescribed fires and agricultural burns
113 are a common land management tool used to improve ecosystem health or facilitate planting crops (Wiedinmyer
114 and Hurteau, 2010; Cochrane et al., 2012). Since prescribed fires in the southeast currently account for about 25
115 thousand km² per year on average (National Interagency Fire Center), it is also important to characterize their
116 emissions.

117 While wildfires and prescribed fires are favorable for many ecosystem functions, the atmospheric impacts of fire on
118 climate, air quality, and health are a major concern. Particles directly emitted or formed via chemical processes have
119 direct and indirect effects on climate by influencing the regional and global radiation balance and impacting cloud
120 properties and precipitation (Braga et al., 2017; Cecchini et al., 2017; Hamilton et al., 2018; Thornhill et al., 2018;
121 Kodros et al., 2020). Global mortality from outdoor pollution due to biomass burning smoke accounts for 600,000
122 premature deaths per year (Johnston et al., 2012), with particulate matter (PM) and O₃ posing the greatest risk factors
123 (Akagi et al., 2014; Dennekamp et al., 2015; Brey and Fischer, 2015; Knorr et al., 2017; Apte et al., 2018). In smoke
124 plumes, O₃ and secondary organic aerosols are photochemically produced from the interplay of NO_x, NMOGs, and
125 meteorology (Tsimplidi et al., 2017; Hodshire et al., 2019). An essential first step to elucidate the factors contributing
126 to PM and O₃ pollution downwind fires is to quantify primary gas- and particle-phase emissions.

127 Numerous studies have quantified emission factors (EFs; grams emitted per kg of dry fuel burned) for various fuel
128 types and different fire characteristics using ground-based or airborne measurements in close proximity to
129 wildland/prescribed fire plumes (e.g., Stockwell et al., 2016; Liu et al., 2017; Peng et al., 2020; Mouat et al., 2022;
130 Lindaas et al., 2021; Permar et al., 2021) or controlled laboratory burns (e.g., Stockwell et al., 2014; Koss et al.,
131 2018; Selimovic et al., 2018). Literature reviews to combine these results have been periodically conducted (Andreae
132 and Merlet, 2001; Akagi et al., 2011; Andreae, 2019), with the most recent by Prichard et al. (2020). Nevertheless,
133 uncertainties in the process-level understanding and model representation of fire emissions, plume rise, and
134 chemistry still exist, which influence model performance in accurately capturing downwind O₃ and secondary
135 organic aerosol formation (Müller et al., 2016; Reddington et al., 2016; Shrivastava et al., 2017). These uncertainties
136 can result from an insufficient understanding of the chemistry and total emissions of NO_x and NMOGs across fuel
137 types, ecosystems, and fire combustion conditions (Warneke et al., 2011; Yokelson et al., 2013; Hatch et al., 2017).

138 In this study, we calculate western US wildfire emission factors for a broad range of gas- and particle-phase species
139 measured aboard the NASA DC-8 during the 2019 Fire Influence on Regional to Global Environments and Air
140 Quality (FIREX-AQ) campaign, which included the most comprehensive payload to date for airborne sampling of
141 biomass burning emissions. We compare our results to the most recent laboratory and airborne field studies,
142 including the fire sciences laboratory component of FIREX-AQ (hereafter referred to as FireLab) (Koss et al., 2018),
143 the fourth Fire Lab at Missoula Experiment, FLAME-4 (Stockwell et al., 2015), the Western Wildfire Experiment
144 for Cloud Chemistry, Aerosol Absorption, and Nitrogen, WE-CAN (Permar et al., 2021), and the Studies of

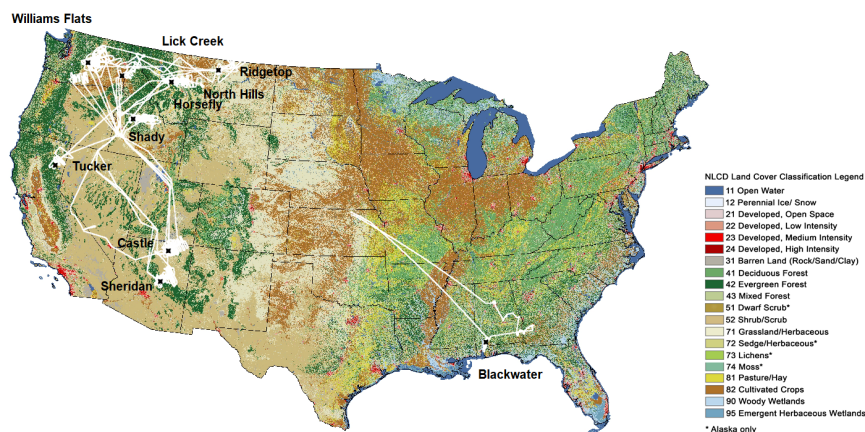
Deleted: 2021

146 Emissions and Atmospheric Composition, Clouds and Climate Coupling by Regional Surveys, SEAC⁴RS (Liu et
147 al., 2017; Wolfe et al., 2022), as well as results summarised in the review by Andreae (2019). We parameterize
148 wildfire emissions based on correlations of carbon- and nitrogen-containing species to CO, NO₂, black carbon, and
149 modified combustion efficiency (MCE) to improve future modeling efforts to accurately capture the chemical
150 evolution of wildfire smoke.

151 2 Methods

152 2.1 Platforms and Instrumentation

153 The NASA DC-8 aircraft was deployed with an extensive suite of instruments to measure the gas- and particle-
154 phase pollutants emitted and photochemically produced downwind of US wildfires. Figure 1 and Table 1 show the
155 research flights analyzed here to capture freshly emitted wildfire smoke from 22 July to 3 September 2019. In total,
156 16 crosswind plume transects downwind from 9 western wildfires and 1 eastern prescribed fire are analyzed, which
157 represent a range of fuel types, including timber, grass, dead trees, logging debris, brush, and litter. The transects
158 are selected based on aging proxies to examine emissions with minimal atmospheric processing. The physical age
159 is determined based on transect proximity to the fire, an estimated plume rise time, and wind speed (Holmes et al.,
160 2020) and ranged from 10–153 min (1–40 km) downwind for the plumes described here. The MCE, defined as
161 $\Delta\text{CO}_2/(\Delta\text{CO}_2+\Delta\text{CO})$, is commonly reported to quantify the fire conditions and describes the relative amount of
162 flaming and smoldering combustion (Yokelson et al., 1996). Pure flaming fires have an MCE near 0.99, while
163 smoldering fires vary over a wider range but are most often near 0.8 (Akagi et al., 2011). For the freshest plume
164 crossings, the MCE was on average 0.90 ± 0.04 (range 0.94–0.85), suggesting a mix of flaming and smoldering
165 emissions.



166

167 **Figure 1:** Selected NASA DC-8 flight tracks for sampling the wildfire and prescribed fire plumes during the 2019 FIREX-AQ.
168 Fires discussed in this study are denoted by black markers. The US map is colored by land cover classification.

169 Multiple instruments performed measurements of gas- and particle-phase species summarized in Table 2. The
170 University of Colorado aircraft aerosol mass spectrometer (CU HRAMS, AMS in the following) (Canagaratna et
171 al., 2007; Guo et al., 2021) measured organic aerosol, particulate ammonium, and nitrate (pNO_y) that consisted of
172 inorganic nitrates (pNO₃), organic nitrates (pRONO₂), and nitroaromatics (pArNO₂) (Day et al., 2022). Black carbon
173 aerosol concentration was measured by a Single-Particle Soot Photometer (SP2) and scaled (~10%) to represent the
174 total accumulation-mode (Schwarz et al., 2008). NMOGs were measured by the NOAA proton transfer reaction
175 time-of-flight mass spectrometer (PTR-ToF-MS) (Yuan et al., 2016), two whole-air samplers, namely the NOAA
176 integrated Whole Air Sampler (NOAA iWAS; <10 second sample time) (Lerner et al., 2017) and the University of

Deleted: fast response *in situ*

178
179
180
181
182

California, Irvine Whole Air Sampler (UCI WAS: < 40 second sample time) (Colman et al., 2001; Simpson et al., 2020), the NCAR Trace

Table 1: Freshest plume crossings identified for analysis during FIREX-AQ 2019. Forest and shrubland fuel types were determined using the FCCS database, while cropland fires were classified with the Cropland Data Layer and DC-8 overflight videos (Warneke et al., 2022).

Fire	Transect number	Date and Time, UTC	Fuel Type	Maleic anhydride to furan as an indicator of OH exposure (ppb ppb ⁻¹)	Physical age (s)	MCE
Shady	0	7/25/2019 22:48	Understory: Ponderosa pine, white-Douglas fir, quaking aspen, two-needle pinyon-Utah juniper forest w/ open shrubs, grasses, and timber litter	0.09	1350	0.91
Shady	9	7/25/2019 23:47		0.07	1250	0.90
North Hills	0	7/29/2019 23:21	Savanna: Ponderosa pine savanna, Douglas-fir-Pacific ponderosa pine, ocean spray forest with Idaho fescue-bluebunch wheatgrass	0.13	600	0.86
Tucker	0	7/30/2019 2:40	Shrubland: Sagebrush-greasewood shrubland with open grasses	0.12	1720	0.91
Ridgetop	4	8/2/2019 23:18	Grassland: Bluebunch wheatgrass, bluegrass with sagebrush-greasewood shrubs and savanna	0.14	2620	0.94
Lick Creek	1	8/3/2019 1:13	Forest: Grand-Douglas fir, Pacific ponderosa pine, ocean spray forest	0.15	1500	0.91
Williams Flats	0	8/3/2019 22:22	Grassland: Idaho fescue-bluebunch wheatgrass-cheatgrass, sagebrush shrublands under open Douglas-fir-Pacific ponderosa pine, ocean spray savanna/forest	0.16	890	0.91
Williams Flats	21	8/4/2019 0:41		0.14	6130	0.91
Horsefly	1	8/6/2019 23:20	Forest: Managed: Subalpine-Douglas fir, lodgepole-whitebark-Pacific ponderosa-Mature lodgepole pine, Engelmann spruce oceanspray forest	0.12	3890	0.87
Horsefly	3	8/6/2019 23:28		0.11	6250	0.85
Williams Flats	7	8/9/2019 1:49	Forest: Douglas-fir-Pacific ponderosa pine, ocean spray forest with grassland understory	0.11	5460	0.91
Castle	0	8/13/2019 0:18	Forest: Ponderosa pine, two-needle-pinyon-Utah juniper, Douglas-white fir, Madrean pine-oak, quaking aspen forest	0.15	1540	0.90
Castle	0	8/13/2019 23:17		0.16	9200	0.90
Castle	10	8/14/2019 1:32		0.07	1600	0.88
Sheridan	1	8/17/2019 0:42	Forest: Pinyon-Utah juniper forest with Turbinella oak-alderleaf mountain mahogany shrubland	0.15	1200	0.91
Blackwater River State Forest	8	8/30/2019 17:11	Forest: Prescription, primarily shrubs, grasses and litter from loblolly-longleaf-slash pine, willow-laurel-turkey-water oak, and magnolia forest	0.31	580	0.93

183

Table 2: Descriptions of the instrumentation aboard the NASA DC-8 used in this study.

Species Measured	Technique	Frequency [Hz]	Inlet Setup	Reference
O ₃ , NO, NO ₂ , NO _y	Chemiluminescence	1	PFA, approx. 1 m long, 1 slpm for each species; NO and NO ₂ additionally pass through 50.9 cm ³ quartz cells	Ryerson et al. (2000)

CO ₂ , CO, CH ₄ , H ₂ O	2x Laser Absorption Spectroscopy	1-5	¼ in stainless steel, 2 m long, 3slpm flow	<i>Sachse et al. (1991)</i> <i>Bourgeois et al. (2022)</i>
NH ₃ , speciated hydrocarbons and OVOCs	PTR-ToF-MS	1 (NH ₃) 10 (others)	PFA, 2 m long, ~20 LPM (before Aug 3), ~60 LPM (from Aug 3 onwards), heated to 60°C	<i>Müller et al. (2016)</i> <i>(with modifications)</i>
PAN, PPN, other PANs	Chemical Ionization Mass Spectrometry (CIMS)	1-10	½" FEP tubing	<i>Zheng et al. (2011)</i>
HONO, HCN, HNCO, HCOOH, N ₂ O ₅ , HPMTF, halogenated compounds	Iodide ToF-CIMS	1	PTFE, 1m long, 6 SLPM, heated to 40°C	<i>Veres et al. (2020)</i>
NO	Laser Induced Fluorescence	1	PFA and silcosteel, 1m length, unheated, overflow at 10-20 slm	<i>Rollins et al. (2020)</i>
CH ₂ O, C ₂ H ₆	Laser Absorption Spectroscopy	1	Heated HIAPER Inlet followed by several meters of heated PTFE Teflon tubing	<i>Richter et al. (2015);</i> <i>Fried et al. (2020)</i>
C ₂ -C ₁₀ Alkanes, C ₂ -C ₄ Alkenes, C ₆ -C ₉ Aromatics, C ₁ -C ₅ Alkyl nitrates, etc.	Whole Air Sampling	Up to 168 per flight	stainless steel	<i>Simpson et al. (2001)</i>
Speciated hydrocarbons and OVOCs	H ₃ O ⁺ ToF-CIMS	1-5	PTFE, 1m long, 1-2 LPM, heated to 50°C	<i>Yuan et al. (2016)</i>
C ₂ -C ₁₀ Alkanes, C ₂ -C ₄ Alkenes, C ₆ -C ₉ Aromatics, C ₁ -C ₅ Alkyl nitrates, etc.	Whole Air Sampling	Up to 72 per flight	PFA, 2m Long, ~60 LPM, unheated	<i>Lerner et al. (2017)</i>
C ₃ -C ₁₀ hydrocarbons, C ₁ -C ₇ OVOCs, HCN, CH ₃ CN, halogenated VOCs, etc.	HR-ToF-GC/MS	0.0095	Restek Silcosteel, 2.5 LPM, heated to 40°C	<i>Apel et al. (2010)</i>
CH ₂ O	Laser Induced Fluorescence	1-10	PFA and silcosteel, 1m length, unheated, overflow at 10-20 slm	<i>Cazorla et al. (2015)</i>
H ₂ O ₂ , organic peroxides, organic acids, isoprene oxidation products, etc.	CIMS	1	A glass tube (3 cm ID and 47cm long) coated with a thin layer of (Fluoropel PFC 801A, Cytonix Corp.). The tube is gently heated and the sampling flow rate through the glass tube is >=40 m/s.	<i>Crouse et al. (2006)</i>
glyoxal, methylglyoxal, HONO, NO ₂	Airborne Cavity Enhanced Spectrometer	1	PTFE Teflon, <1 m length, inlet heated to 25°C, 10.5 vlpn	<i>Min et al. (2016)</i>
BC mass concentration	SP2	1	NASA Langley inlet with optional dilution	<i>Schwarz et al. (2008)</i>
Submicron aerosol composition	CU-HR-AMS	1 (up to 10 Hz in plumes)	HIMIL tall inlet, 1.3 m SS 0.18" ID+ 0.45 m 0.08" ID tubing + pressure controlled instrument inlet (<0.3 s total residence time)	<i>Guo et al (2021);</i> <i>Canagaratna et al (2007)</i>

Deleted: teflon

Deleted:

184 Organic Gas Analyzer (Apel et al., 2015), a fast online gas chromatograph outfitted with a Time-of-Flight mass
185 spectrometer (TOGA-TOF; < 35 second sample time), the Caltech chemical ionization time-of-flight mass
186 spectrometer (CIT-ToF-CIMS), and for selected flights the University of Innsbruck / University of Oslo
187 (UIBK/UiO) PTR-ToF-MS (prototype PTR-TOF 4000X2; IONICON Analytik GmbH, Innsbruck, Austria). Three
188 instruments were used in this study that measured formaldehyde: the In Situ Airborne Formaldehyde (ISAF)
189 instrument (Liao et al., 2021), the Compact Atmospheric Multispecies Spectrometer (CAMS) (Weibring et al.,
190 2007), and the UIBK/UiO PTR-ToF-MS. ISAF and CAMS correlated with an R² coefficient of 0.99 and a slope of

193 1.27, as discussed by Liao et al. (2021); whereas the UIBK/UiO PTR-ToF-MS agreed better with the CAMS, with
194 a slope of 1.02. In this study, we use the ISAF measurements, which have the best time response compared to all
195 other instruments and adjust the mixing ratios to match those reported by CAMS and the UIBK/UiO PTR-ToF-MS.
196 The NOAA Iodide ion chemical ionization mass spectrometer (NOAA CIMS) (Veres et al., 2020; [Robinson et al.,
197 2022](#)) was used to measure formic acid (HCOOH), nitrous acid (HONO), and dinitrogen pentoxide (N₂O₅). CO and
198 CH₄ were measured via mid-IR wavelength modulation spectroscopy by the Differential Absorption Carbon
199 Monoxide Measurement (DACOM) instrument (Sachse et al., 1991). CO₂ was measured via nondispersive infrared
200 absorption spectroscopy using a LICOR model 7000 analyzer (Vay et al., 2009). NO, NO₂, and NO_y were measured
201 by the NOAA chemiluminescence instrument (Bourgeois et al., 2020). NO_y measures the sum of reactive nitrogen
202 compounds, including NO, NO₂, HONO, peroxy nitrates, alkyl and multifunctional nitrates, and particulate nitrate.
203 Additional measurements of HONO and NO₂ were provided by the NOAA Airborne Cavity Enhanced Spectrometer
204 (ACES) (Min et al., 2016) and NO by the NOAA Laser Induced Fluorescence instrument (NO-LIF) (Rollins et al.,
205 2020). Glyoxal and methylglyoxal were measured by ACES, and ammonia (NH₃) by the UIBK/UiO PTR-ToF-MS
206 (Müller et al., 2016; Tomsche et al., 2023). The Georgia Tech CIMS (GT-CIMS) was used to measure peroxyacetyl
207 nitrate (PAN) and other PAN-like compounds such as peroxypropionyl nitrate, peroxyacryloyl nitrate, and
208 peroxybutyryl nitrate. Finally, the plume structure was obtained from aerosol backscatter measured with the NASA
209 Langley Airborne Differential Absorption Lidar (DIAL). All measurements reported here are provided in the NASA
210 FIREX-AQ data repository (NASA airborne science data for atmospheric composition, 2019).

211 In this study, we focus on quantifying total and speciated NMOG emissions, which were predominantly measured
212 by PTR-ToF-MS, the two Whole Air Samplers, and [the Trace Organic Gas Analyzer with Time-of-Flight mass
213 spectrometer \(TOGA-TOF\)](#). The same NOAA PTR-ToF-MS and the iWAS systems were used at the US Forest
214 Service's Missoula Fire Sciences Laboratory (FireLab) in 2016 as a precursor to FIREX-AQ and described by Koss
215 et al. (2018). Koss et al. (2018) speciated isomers measured by PTR-ToF-MS using gas chromatography pre-
216 separation and reported isomer distributions for over 150 individual masses. Here, we compare these isomer
217 distributions to the speciation derived based on the comparison of the GC-MS and PTR-ToF-MS measurements
218 conducted aboard the NASA DC-8 (Table S5). Two calibration methods were used to determine NMOG sensitivities
219 for the PTR-ToF-MS. For commercially available compounds, sensitivities were determined by gravimetrically
220 prepared standards or by liquid calibration, as described by Coggon et al. (2019). Sensitivities for other species were
221 estimated based on calculated proton transfer rate coefficients, as described by Sekimoto et al. (2017). For the WAS
222 system(s), NMOGs were calibrated using gravimetrically prepared standards, as described by Lerner et al. (2017).
223 A detailed description of the PTR-ToF-MS and WAS setups as well as NMOG uncertainty is included in the
224 supplement.

225 **3 Results and discussion**

226 **3.1 Plumes with minimal photochemical aging**

227 Emissions from wildfire plumes chemically transform once injected into the atmosphere (e.g., Akagi 2012;
228 Robinson et al., 2021; Decker et al., 2021; Xu et al., 2021). However, safety and operational constraints limit the
229 proximity of airborne sampling to the fire. An essential first step to quantifying wildfire primary emissions is to
230 identify plume samples that have undergone minimal chemical processing. Commonly, the freshest plumes are
231 identified using the plume age calculated from the distance downwind of the wildfire using the onboard measured
232 average wind speed (e.g., Permar et al., 2021) but neglecting plume rise. The physical age does not necessarily
233 identify plume crossings with the least chemical processing since the sampled smoke can be impacted by
234 meteorology, solar radiation, radical concentrations, and sampling artifacts related to the aircraft's position relative
235 to the center of the plume (Robinson et al., 2021; Decker et al., 2021; Wang et al., 2021).

236 Here, we account for oxidation by hydroxyl radical (OH) using the ratio of primary and secondary NMOG wildfire
237 tracers, specifically furan (a primary species; Koss et al., 2018) and maleic anhydride (a slow-reacting, secondary
238 species observed downwind of fires) (Zhao and Wang, 2017). Coggon et al. (2019) show that maleic anhydride
239 quickly forms downwind of fires from the OH oxidation of furans, and Wang et al. (2021) show that the distribution
240 of maleic anhydride in plumes closely mirrors the distribution of OH exposure. Since furan is a direct wildfire
241 emission and maleic anhydride is a chemical product of furan chemistry that is not significantly emitted from fires

(Coggon et al., 2019; Wang et al., 2021), the ratio of maleic anhydride to furan (MA/F) is expected to increase downwind of a fire and exhibit a minimum in the least-processed plumes. This ratio is used as a photochemical proxy to identify the freshest sampled plumes by extracting the lowest MA/F transect per wildfire plume and reduce the effects of chemical degradation on our primary NMOG emission calculations. We note that this technique may not account for the faster photolysis of light-absorbing species (such as HONO) or fast interconversion between NO and NO₂, though the sum of reactive nitrogen species (NO_x) is expected to be conserved downwind of fires (Lindaas et al., 2020). We note that a quantitative relationship between MA/F and OH exposure is not presented here as the yield of maleic anhydride from furan oxidation requires further laboratory quantification. Other furans also produce maleic anhydride (Coggon et al., 2019), and thus the MA/F ratios used here is simply a proxy for screening out significantly processed emissions.

Figure 2a shows the maleic anhydride, furan, and CO concentration downwind of the Williams Flats wildfire on 3 August 2019, as a characteristic example. Figure 2b shows the relationship between maleic anhydride and furan for all of the plume-crossings sampled during FIREX-AQ. The freshest crossings for each fire are highlighted as circles colored by the estimated smoke age. Also shown are the MA/F and the median physical smoke age calculated for each plume crossing. Here we use the high time resolution of PTR-ToF-MS for MA and furan concentrations, but furan is additionally scaled by 0.46 to match the TOGA GC-MS concentrations as discussed in Sect. 3.2. VOC and CO concentrations were highest closer to the wildfire and decreased downwind, primarily due to dilution. During the Williams Flats (Fig. 2a), the MA/F increased from 0.20 to 0.86 downwind of the fire, indicating active chemical conversion of furan to maleic anhydride. The physical smoke age followed the same increase from 0.5 to 4 hours. Figure 2b shows that the MA/F for all of the freshest plume crossings had a median of 0.13 (0.10–0.16, 25th–75th), and their corresponding physical age was less than 1.46 h (0.6–1.74) (see Table 1). It is notable that certain fires with similar MA/F ratios ranged in physical age from 15 minutes to as high as 3–4 hours. These differences show how chemical processing in some plumes may be slow over long-distances, while other plumes may undergo immediate oxidation. Despite these differences, the majority of chemically fresh plumes sampled during FIREX-AQ exhibited very similar MA/F ratios (Fig. 2b).

Deleted: clock

Deleted: but that

Deleted: Also

Deleted: ,

Deleted: 3,

Deleted: The

Deleted: wildfire plumes and the extracted freshest plume crossings. The freshest plume crossings

Deleted: MA/F

Deleted: However

Deleted: ,

Deleted: drastically

267

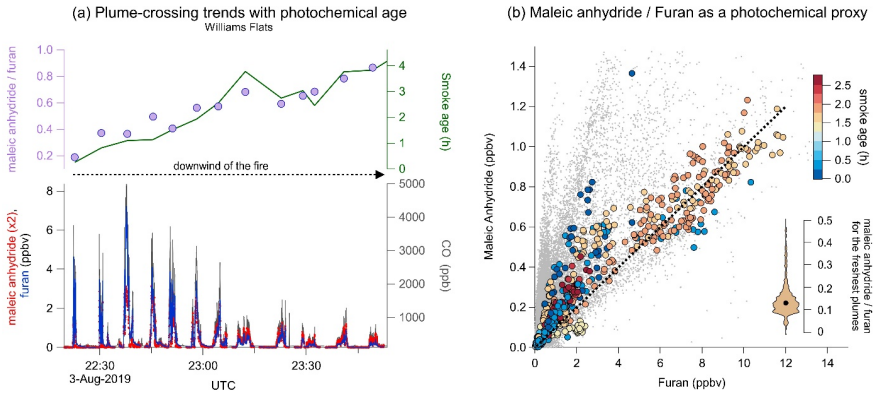


Figure 2: (a) Mixing ratios of maleic anhydride, furan, and CO (bottom) and ratios of maleic anhydride to furan (top) in 12 crosswind plume transects of smoke from the Williams Flats fire on 3 August 2019. The maleic anhydride to furan ratio increases as the plume ages during transport away from the Williams Flats. (b) Comparison of the maleic anhydride and furan mixing ratios used as a photochemical proxy to identify the freshest plume crossings during FIREX-AQ. Grey points are all 1-second resolution measurements during FIREX-AQ, and circles are the chosen freshest plume crossings colored by the physical smoke age. The violin plot shows the variability of the ratio of maleic anhydride to furan for the freshest wildfire transects.

Deleted: clock

Figure S1 further highlights differences in the physical and chemical age of a fire by focusing on the Williams Flats wildfire and the Blackwater prescribed fire. The DIAL image shows the shape and evolution of the wildfire smoke from overpass flights. For the Williams Flats fire, the DC-8 sampled emissions by performing raster patterns

290 perpendicular to the smoke, whereas for the Blackwater fire, the DC-8 also flew along the smoke plume at various
291 altitudes. For the Blackwater fire, the MA/F increased rapidly up to 1.4 ppbv ppbv⁻¹ 30 km downwind of the wildfire,
292 while for the Williams Flats fire, the ratio reached a maximum of 1 ppbv ppbv⁻¹ 120 km downwind of the fire. These
293 differences further highlight the importance of accounting for the chemical rather than the physical age of a fire to
294 determine the freshest transects.

295 The MA/F for fresh, unaged smoke during the FireLab study was ~ 0.04 ppbv ppbv⁻¹ (Wang et al., 2021), showing
296 that even the freshest plume transects sampled during FIREX-AQ were photochemically processed to some extent.
297 For the remainder of this analysis, fire plumes sampled closest to the emission source that exhibited a MA/F > 0.20
298 are excluded from the calculation of emission ratios and enhancements. This cut-off is based on the median MA/F
299 ratio observed for the freshest plume plumes sampled during FIREX-AQ (0.13 ppbv ppbv⁻¹, Fig. 2b). The exception
300 is the Blackwater prescribed fire that was the only fire representative of southeastern US fuel types included in our
301 analysis, even though the freshest plume crossing had a MA/F of 0.3. Further evaluation of biases during FIREX-
302 AQ for fast-reacting species is discussed in Sect. 3.3.

303 3.2 Instrument comparisons

304 NMOG measurements obtained from the NOAA PTR-ToF-MS were compared to other instruments onboard the
305 DC-8, including TOGA-TOF, 2 WAS systems, CIT-CIMS, UIBK/UiO PTR-ToF-MS, and NOAA CIMS. Table S5
306 provides correlations of the PTR-ToF-MS measurements to other instruments. For calibrated compounds, the
307 NOAA PTR-ToF-MS and the UIBK/UiO PTR-ToF-MS agreed within 10–35% for methanol, acetonitrile, acetone,
308 methyl ethyl ketone (MEK), benzene, toluene, C₈ and C₉ aromatics, and monoterpenes. The NOAA PTR-ToF-MS,
309 and NOAA CIMS agreed within uncertainty for hydrogen cyanide (HCN), isocyanic acid (HNCO), and formic acid,
310 respectively. CIT-CIMS agreed with the NOAA PTR-ToF-MS for HCN whereas for phenol it was lower by a factor
311 2. Both instruments were calibrated for phenol suggesting that differences could be due to PTR-ToF-MS
312 fragmentation of higher molecular weight gases that produce signals at the phenol ion mass, or differences in the
313 detection of other isomers from the two instruments.

314 Although the PTR-ToF-MS provides high time resolution measurements, it cannot speciate NMOG isomers detected
315 at the same exact mass. In the following, we compare mixing ratios derived for the PTR-ToF-MS chemical formula
316 to the combined isomer signals derived from GC-MS, given in parentheses. When compared to the iWAS, WAS,
317 and TOGA-TOF measurements, the NOAA PTR-ToF-MS was within ±25–35% for CH₄O (methanol), C₂H₃N
318 (acetonitrile), C₂H₄O (acetaldehyde), C₂H₆O (ethanol), C₆H₆ (benzene), C₇H₈ (toluene), C₃H₃N (acrylonitrile),
319 C₃H₄O (acrolein), C₃H₆O (acetone + propanal), C₈H₁₀ (ethylbenzene + m-, p-, and o-xylenes), and C₄H₆O (methyl
320 vinyl ketone + methacrolein + 2-butenal). However, the NOAA PTR-ToF-MS was higher by a factor of 2 or more
321 for C₂H₆S (dimethyl sulfide), C₄H₅N (pyrrole + butene nitrile isomers), C₄H₄O (furan), C₃H₆O₂ (methyl acetate +
322 ethyl formate + hydroxyacetone), C₅H₆O (2-methyl-furan + 3-methyl-furan), C₅H₄O₂ (furfural + 3-furaldehyde),
323 and C₁₀H₁₆ (monoterpenes) whereas CH₃NO₂ (nitromethane) agreed with the WAS but was lower than TOGA-TOF.

324 The discrepancies between the GC-MS techniques and PTR-ToF-MS for a number of key species, such as furans,
325 generally show that the PTR-ToF-MS measures more signal than what can be accounted for by GC-MS. This
326 observation likely results from a combination of (a) PTR-ToF-MS fragmentation of higher molecular weight gases
327 that produce signals at parent ion masses, (b) the detection of isomers that cannot elute through a GC column, and
328 (c) the detection of molecules that are lost to canister sampling. To investigate the causes of these discrepancies,
329 Table S5 shows isomer distributions for masses detected by the PTR-ToF-MS that are known to represent the sum
330 of two or more overlapping isomers. These isomer distributions are calculated from the ratio of GC-MS
331 measurements to the corresponding PTR-ToF-MS mass. Each ratio represents the fraction of the total signal
332 measured by PTR-ToF-MS that is associated with a given isomer. For example, GC-MS measurements identify 2-
333 methylfuran and 3-methylfuran as the key isomers with the molecular formula C₅H₆O. The slope of isomers to PTR-
334 ToF-MS measurements of C₅H₆O represents the isomer fraction detected by PTR-ToF-MS.

335 The isomer distributions shown in Table S5 are compared to those reported for laboratory smoke by Koss et
336 al. (2018). Koss et al. (2018) assigned PTR-ToF-MS masses based on literature searches, intercomparisons of PTR-
337 ToF-MS measurements to other in situ instrumentation, and offline analysis by coupling GC effluent of sampled

Deleted: partially

Deleted: with a median MA/F that was 0.14 ppbv ppbv⁻¹.
F...

Deleted: showed

Deleted: significant chemical processing with

Deleted: this

Deleted: analysis

Deleted: methyl

Deleted: methyl

347 smoke to the inlet of the PTR-ToF-MS (combined instrumental setup termed GC-PTR-ToF-MS). For low molecular
348 weight gases known to elute through a GC column, Koss et al. (2018) assigned isomer distributions based on the
349 total signal detected by GC-PTR-ToF-MS, which includes signals from parent ions produced from proton-transfer
350 as well as fragments from higher molecular weight gases that elute through a GC. For example, at $C_5H_6O-H^+$ (m/z
351 83.0491), 51% of the signal resulted from the elution of 2-methylfuran, 9% resulted from 3-methylfuran, and 37%
352 was associated with other peaks in the chromatogram that produced signals at $C_5H_6O-H^+$ (unidentified isomers +
353 fragments of higher masses). We note that the PTR-ToF-MS instrument employed in this study is the same as that
354 used by Koss et al. (2018) and is operated with the same drift field ($E/N = 120$ Td).

355 For species measured during FIREX-AQ where the PTR-ToF-MS reported significantly more mass than the GC
356 instruments, we find that the isomer distributions derived in this study significantly differ from those derived by
357 Koss et al (2018) (Table S5). This is most pronounced for the monoterpenes but also the furanoic species, such as
358 furan (C_4H_4O), methylfurans (C_5H_6O), and furfurals ($C_5H_4O_2$). Hatch et al. (2017) showed that more than 30
359 different isomers can contribute to the monoterpenes signal based on two dimensional GC. However, the
360 conventional GC instruments used during FIREX-AQ could only detect a fraction of these isomers. Furthermore,
361 differences in sensitivity for the different isomers would further increase the quantification uncertainties for both
362 GC and PTR-ToF-MS. For the furanoic masses, the PTR-ToF-MS measures a higher fraction of unknown isomers
363 and fragments than what is reported by Koss et al. (2018). This result holds whether comparing against isomer
364 distributions derived using TOGA (an online GC method) or WAS methods (a canister sampling method),
365 suggesting that uncertainties due to differences in calibration are small. These results suggest that the total signal of
366 furans measured by PTR-ToF-MS during FIREX-AQ is likely influenced by gases that cannot pass through a GC
367 column, which includes the possibility of unidentified isomers and fragments from higher molecular weight species.
368 We note that this result is not specific to the PTR-ToF-MS used in this study, as the agreement between the NOAA
369 PTR-ToF-MS and UIBK/UiO PTR-ToF-MS for these masses is within 3% (Table S5).

370 Furans are an important contributor to VOC reactivity and significantly contribute to the formation of ozone and
371 other secondary gases (Gilman et al., 2015; Hatch et al., 2017; Coggon et al., 2018). For models employing emission
372 factors of furans, we recommend using emission factors derived using GC-based methods given that multiple
373 isomers can be detected with PTR-TOF-MS at the furan mass. This also applies to other specific compound classes.
374 In Table S1, we include the methods used in this study to derive emission factors. For applications where the fast
375 time-resolution from PTR-ToF-MS is needed (e.g., in deriving cross-plume trends in gases), (Decker et al. 2021; Xu
376 et al. 2021), the interpretation of trends in furans should include the possibility of unknown isomers and fragments.

377 3.3 Emission ratios and emission factors of US wildfire smoke

378 The freshest plume transects are used to estimate the primary emissions for individual fires. Table 3 shows the
379 average compound-specific enhancement ratios to CO which we interpret as emission ratios (ERs) for most species,
380 and the inferred emission factors (EFs) calculated for more than 100 species and groups of species from the freshest
381 wildfire plume transects sampled during FIREX-AQ. ERs and EFs for each fire are also calculated and provided in
382 Tables S2 and S3. Given that fast chemistry already occurred in some fire transects, the ER and EF estimates of
383 highly reactive species like HONO are lower bounds. ERs are the slope of a linear fit of each species with CO
384 mixing ratios (see Sect. S1). EFs were calculated following Eq. (1):

$$385 EF_i = F_C \cdot \frac{MM_i}{AW_C} \cdot \frac{\Delta i/\Delta CO}{\sum_{x=1}^n (NC_x \cdot \frac{\Delta C_x}{\Delta CO})}, \quad (1)$$

386 where EF_i is the emission factor of compound i calculated similarly to Akagi et al. (2011); F_C is the carbon fraction
387 of the fuel assumed to be 0.5 g g^{-1} ; MM_i is the molar mass of i ; AW_C is the atomic mass of carbon (12 g mol^{-1});
388 $\Delta i/\Delta CO$ is the emission ratio of a compound relative to CO; NC_x is the number of carbon atoms in C-containing
389 species x , and $\Delta C_x/\Delta CO$ is the emission ratio of species x to CO. This method assumes that all the carbon lost from
390 the fuel as it burns is emitted and measured, which is a reasonable approximation as CO, CO₂, and CH₄ account for
391 most of the emitted carbon (Akagi et al., 2011). The denominator of the last term estimates total carbon relative to
392 CO. Species C_x includes all species shown in Table 3. The carbon not quantified by the suite of instrumentation

Deleted: or canister effects

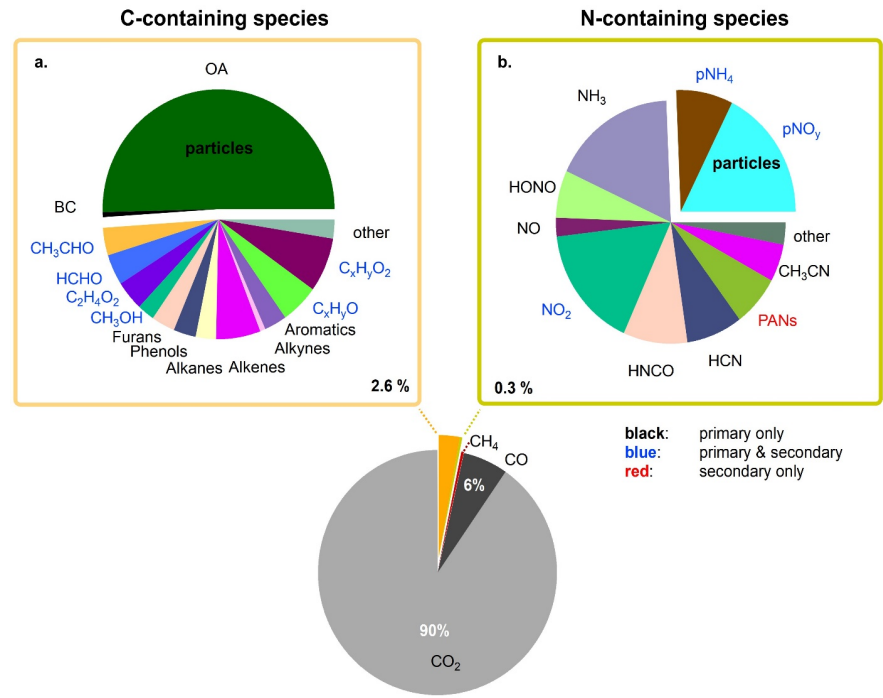
Deleted: ,

Deleted: ,

Deleted: section

397 available during FIREX-AQ likely results in emission factor overestimates no more than 1–2% (Yokelson et al.,
 398 2013; Stockwell et al., 2015).

399 Figure 3 shows the average chemical composition of freshly emitted wildfire smoke in g kg^{-1} (see Eq. (1)). CO_2 ,
 400 CO , and CH_4 are 97% of the total mass. The remaining 3% consisted of gas- and particle-phase carbon-containing
 401 (C-containing, 2.6%) and nitrogen-containing (N-containing, 0.3%) species. 50.4% and 0.7% of this remaining C-
 402 containing total mass results from organic aerosol and black carbon (BC), respectively. In the gas phase, 6.4% of
 403 the remaining C-containing species mass, which includes all species in Fig. 3a, were phenolic compounds and
 404 furans, 4% formaldehyde (HCHO), 4% glycolaldehyde and acetic acid ($\text{C}_2\text{H}_4\text{O}_2$), 3.7% acetaldehyde (CH_3CHO),
 405 2.1% methanol, 5.8% remaining compounds with one oxygen atom ($\text{C}_x\text{H}_y\text{O}$), 6.9% remaining compounds with two
 406 oxygen atoms ($\text{C}_x\text{H}_y\text{O}_2$), 3.1% aromatics, 6.3% alkenes, 2.8% alkanes, and 3.3% other species. N-containing species
 407 mass, shown in Fig. 3b, consisted of organic and inorganic nitrate, and other organic nitro compounds such as
 408 nitroaromatics (pNO_y , 19%) and ammonium (pNH_4^+ , 8.5%) in the particle-phase; whereas, the dominant gas-phase
 409 N-containing species mass was from ammonia (NH_3 , 18.5%), followed by nitrogen dioxide (NO_2 , 17.5%), isocyanic
 410 acid (HNCO, 8.5%), hydrogen cyanide (HCN, 5%), peroxyacyl nitrates (PANs, 7%), nitrous acid (HONO, 4.8%),
 411 nitric oxide (NO, 2.5%), and others at 3%. The high contribution of NO_2 in comparison to NO and HONO, and the
 412 existence of secondary pollutants, in particular PANs, also indicate that chemistry occurred from the time of
 413 emission to the time of detection. Given the fast conversion of NO and HONO to NO_2 and nitrate, and NH_3 to
 414 particulate ammonium, we also include in Table 3 the conserved quantity of NO_y , as well as NO_x as NO, and NH_x
 415 as NH_3 + particulate ammonium. Emissions of SO_x as SO_2 that include the conversion of SO_2 to particulate sulfate
 416 are discussed in Rickly et al. (2022).



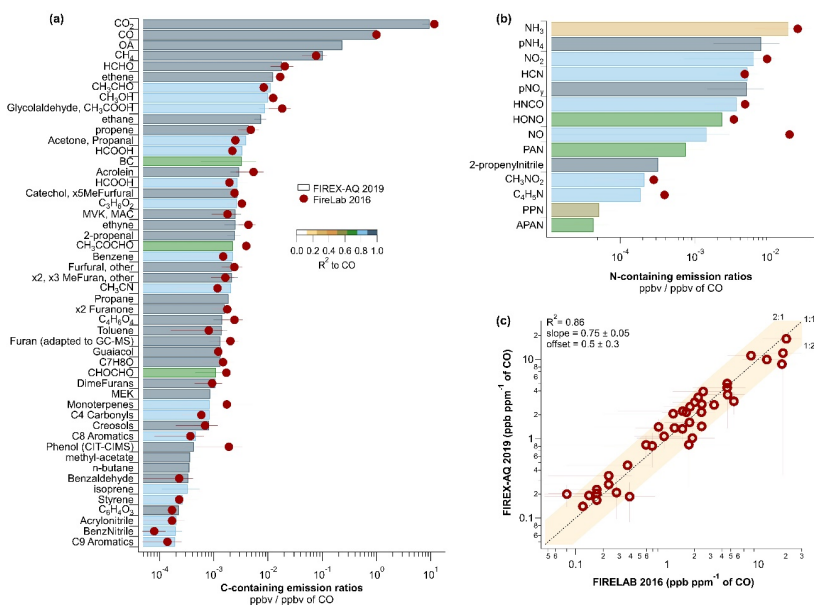
417 **Figure 3:** Pie charts of carbon- and nitrogen-containing species average emission factors (g kg^{-1}) for fresh wildfire smoke. The
 418

421 text labels indicate compounds with only direct emissions in black, and compounds that are directly emitted and photochemically
 422 produced in blue, and PANs that are only photochemically produced in red, indicating some oxidation even for the freshest
 423 plumes sampled. Although HCHO and CH₃CHO are C_xH_yO species and glycolaldehyde/acetic acid are C_xH_yO₂ species they are
 424 separately presented due to their high abundances.

425 **3.4 FIREX-AQ field observations compared to laboratory and field studies**

426 The sum of the NMOG EFs sampled during the FIREX-AQ campaign was $26.88 \pm 8.5 \text{ g kg}^{-1}$ (3σ), in agreement
 427 with the mean sum from western wildfires during the WE-CAN campaign of $26.1 \pm 6.9 \text{ g kg}^{-1}$ (Permar et al., 2021),
 428 temperate forest fires at 23.7 g kg^{-1} (Akagi et al., 2011) and 24.55 g kg^{-1} (Andreae, 2019), pine-forest understory
 429 prescribed fires at 27.6 g kg^{-1} (Yokelson et al., 2013), FLAME-4 laboratory coniferous canopy fires at 23.9 g kg^{-1}
 430 (Stockwell et al., 2015), and FireLab laboratory measurements of various different fuel types at 25 g kg^{-1} (Koss et
 431 al., 2018). The sum of FIREX-AQ NMOG ERs to CO on a molar basis was $134.2 \pm 20 \text{ ppb ppm}^{-1}$, in a similar range
 432 as WE-CAN at $148.3 \pm 29.6 \text{ ppb ppm}^{-1}$ and FireLab at $144.5 \text{ ppb ppm}^{-1}$.

Deleted: 23.80
 Deleted: 7
 Deleted: 135
 Deleted: 18



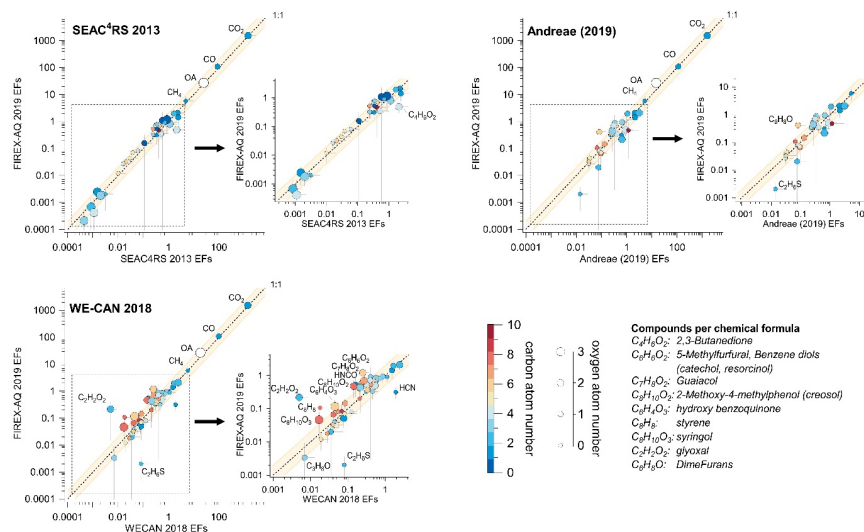
433 **Figure 4:** (a) and (b) show the emission ratios for FIREX-AQ (bars) and FireLab (circles) colored by the correlation coefficient,
 434 and (c) direct comparison of FIREX-AQ to FireLab emission ratios for gas-phase species. Error bars in all graphs indicate the 1-
 435 sigma standard deviation. The majority of the observations from FireLab 2016 were calculated using data from the NOAA PTR-
 436 ToF-MS; here we use measurements from the same instrument for FIREX-AQ for more direct comparisons.
 437

438 Figure 4 compares the ERs of C-containing and N-containing compounds (ppb ppb⁻¹ CO) with those measured at
 439 the FireLab (Koss et al., 2018; Selimovic et al., 2018). During FIREX-AQ, all NMOGs correlated well with CO
 440 with correlation coefficients, R² above 0.75, confirming that CO could be used as a proxy for estimating NMOG
 441 emissions close to the fire, as further discussed in Sect. 3.5. Variability in the correlations of individual species with
 442 CO was still evident — for example, species that are both emitted and photochemically produced exhibited lower
 443 correlation (e.g., acetic acid, acetone, and formic acid, R² = 0.75–0.85) than compounds with only primary emissions
 444 from fires (e.g., aromatics, R² > 0.95). N-containing species were weakly correlated with CO partly due to varying
 445 fuel N/C (Roberts et al., 2020). In addition, lower correlation of NH₃ could be due to variable amounts of ammonium
 446 formation in aging smoke, or differences in instrument response times between a high volatility compound, such as
 447 CO, compared to NH₃, which may partition to the inlet and instrument walls before detection (Tomsche et al., 2023;

Deleted: ,
 Deleted: ,

454 Stockwell et al., 2014) and slow the instrument response time. Low correlations are also found for HONO, which is
 455 highly reactive and removed by photochemistry (Peng et al., 2020; Theys et al., 2020), as well as for glyoxal and
 456 methylglyoxal, which are photochemically formed and could partition differently to the particle phase depending on
 457 humidity (Mitsubishi et al., 2018; Ling et al., 2020). N-containing species were in good agreement except the higher
 458 contribution of NO and particulate ammonium in Firelab and FIREX-AQ, respectively. This difference reflects the
 459 depletion of NO and the secondary formation of particulate ammonium in field observations and promotes that fast
 460 chemistry of reactive compounds occurred prior to the FIREX-AQ sampling. In summary, variability in post-
 461 emission processes, fuel nitrogen, and fast photochemistry are likely important factors that contribute to the
 462 differences in correlations between FIREX-AQ and Firelab measurements of NMOGs, NO_y species, and CO.

463 While the PTR-ToF-MS is well-suited for detecting NMOGs, it is prone to fragmentation for a range of molecules,
 464 depending on their molecular structure (Pagonis et al., 2019). For such compounds, measurement uncertainties
 465 increase, and comparisons to previous studies that use different instrumentation become more challenging. As
 466 outlined in Sect. 2, the NOAA PTR-ToF-MS used in this study was the same instrument as used in the FireLab three
 467 years prior (Koss et al., 2018). This provided an important opportunity to compare field-derived emissions to
 468 laboratory studies. FireLab average ERs were calculated by comparing similar fuel types as measured during
 469 FIREX-AQ, including ponderosa pine, lodgepole pine, Douglas fir, subalpine fir, engelmann spruce, loblolly pine,
 470 jeffrey pine, juniper, manzanita, chamise, and bear grass laboratory burns. Overall, FIREX-AQ ERs agree with those
 471 from the FireLab within a factor of 2 for most compounds (see Fig. S3). Compounds with the largest differences
 472 were benzonitrile with a FIREX-AQ to FireLab ratio of 2.46, ethene (1.88), CH₃CN (1.77), toluene (1.71), HCOOH
 473 (1.64), the sum of acetone and propanal (1.62), glycolaldehyde and acetic acid (0.50), monoterpenes (0.49), C₄H₅N
 474 species (0.47), syringol (0.32), and ethanol (0.28).



476 **Figure 5:** Comparison of FIREX-AQ EFs to those from SEAC⁴RS 2013 (Liu et al., 2017), WE-CAN 2018 (Permar et al., 2021),
 477 and the review publication by Andreae (2019). Shaded areas show differences within a factor of 2.

478 Figure 5 and Table S6 compare FIREX-AQ observations against field-derived wildfire EFs from SEAC⁴RS (Liu et
 479 al., 2017), WE-CAN (Permar et al., 2021), and literature-average temperate forest EFs from Andreae (2019). For all
 480 studies, the measurements agree within a factor of 2 for 83%, 87%, and 78% of the compounds reported during
 481 SEAC⁴RS, WE-CAN, and the Andreae (2019) temperate forest fires average (includes SEAC⁴RS), respectively.
 482 FIREX-AQ EFs were on average higher compared to previous studies. The average ratio ($\pm 1\sigma$) of FIREX-AQ to
 483 WE-CAN, SEAC⁴RS, and temperate forest fires from Andreae (2019) were 1.42 ± 0.3 , 1.26 ± 0.42 , and 1.24 ± 0.36 ,

- Deleted: Ponderosa
- Deleted: Pine
- Deleted: Lodgepole
- Deleted: Pine
- Deleted: Fir
- Deleted: Subalpine
- Deleted: Fir
- Deleted: Engelmann
- Deleted: Spruce
- Deleted: Loblolly
- Deleted: Pine
- Deleted: Jeffrey
- Deleted: Pine
- Deleted: Juniper
- Deleted: Manzanita
- Deleted: Chamise
- Deleted: Bear
- Deleted: Grass
- Deleted: fires
- Deleted: Figure

504 respectively (see Table S6). Glyoxal and methylglyoxal were expected to have higher discrepancies due to their
505 secondary production and RH-dependent particle-phase partitioning, but also due to the higher quantification
506 uncertainties in the previous studies. For example, during WE-CAN (Permar et al., 2021), a PTR-ToF-MS was used
507 to detect these compounds, which are prone to fragmentation upon ionization in the PTR-ToF-MS. Furthermore, the
508 calculated glyoxal sensitivity used by Permar et al. (2021) was high (Stöner et al., 2016) and could therefore lead
509 to a significant underestimation. In this study, glyoxal and methylglyoxal were measured by cavity-enhanced
510 spectroscopy, and the uncertainties were < 5% (see Sect. 2). Furthermore, comparison of the FIREX-AQ to the
511 FireLab EFs also measured by the same spectroscopic technique (see Fig. 4) (Zarzana et al., 2018) showed that
512 glyoxal and methylglyoxal were in better agreement with FIREX-AQ compared to Permar et al. (2021) but still
513 lower by 50% and 75%, respectively. Dimethyl sulfide (DMS) is a compound that originates predominantly from
514 oceanic emissions and its fire emissions were lower for this study compared to WE-CAN and the temperate forest
515 fire emissions average, but higher by 20% compared to the SEAC⁴RS EFs. FIREX-AQ monoterpenes were higher
516 than those in WE-CAN and Firelab by a factor of 2, and lower than the temperate forest fire emissions average
517 (Andreae 2019) by a factor of 2, which likely stems from the large variability of monoterpene emissions for different
518 fuel types and the difficulties inherent with the large number of isomers (Hatch et al., 2017; Koss et al., 2018;
519 Sekimoto et al., 2018). OA was 50% higher compared to WE-CAN and temperate forest fire emissions, but within
520 10% when compared to the SEAC⁴RS OA emissions. Some of the OA estimates that went into the Andreae (2019)
521 averaged OA EF value were calculated from OC with an assumed OA:OC value of 1.6, lower than the value of 1.89
522 used in this work (Table 3); while a correction of Andreae's data is not possible since it is not transparent which
523 studies included in that compilation are affected, this will result in a small high bias in O:C The variability of OA
524 EFs highlights the importance of accounting for the partitioning and aging of OA when comparing OA EFs across
525 biomass burning campaigns given that fraction of the detected OA from wildfire plumes can be a mix of primary
526 and secondary (Pagonis et al., 2020).

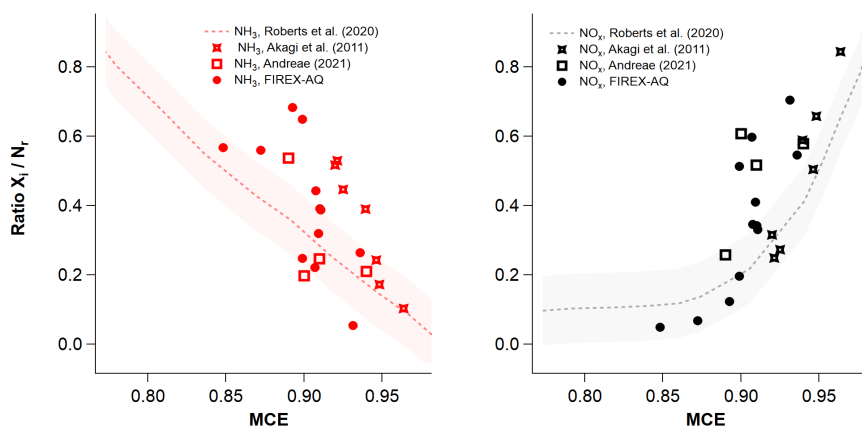
Deleted: ure

527 Focusing on the two large recent campaigns dedicated to wildfires we note that differences can occur due to natural
528 variability with 2018 being a more intense fire season (Jin et al., 2023), but also from the different fragmentation,
529 inlet setups, and quantification uncertainties between the instruments used. Differences between the WE-CAN and
530 FIREX-AQ EFs for oxygenated compounds could be due to the different quantification uncertainties between the
531 two PTR-ToF-MS instruments. For both studies and instruments, assuming similar isomer sensitivities and no
532 fragmentation interferences, sensitivities for calibrated compounds introduced a 15% uncertainty, whereas
533 sensitivities for uncalibrated species were estimated following theoretical methods described by Sekimoto et al.
534 (2017), which have an uncertainty of 50%. Several reactive oxygenated compounds that have implications for NO_x
535 loss processes such as the formation of nitrophenolic compounds (Finewax et al., 2018; Decker et al., 2021) were
536 calibrated during FIREX-AQ but only calculated during WE-CAN, such as C₇H₈O (o-cresol, anisol), C₇H₈O₂
537 (guaiacol), and C₈H₁₀O₂ (creosol). One mass calibrated on both instruments was C₆H₆O₂ (sum of 5-methyl-furfural,
538 catechol, and resorcinol), but was still a factor of 5 higher during FIREX-AQ compared to WE-CAN. However, the
539 FIREX-AQ ERs for C₆H₆O₂ agreed within 45% of the FireLab study, which used the same instrument, suggesting
540 possible differences in fragmentation or isomer assignment between the FIREX-AQ and WE-CAN instruments.
541 Styrene (C₈H₈) from FIREX-AQ (using PTR-MS) was a factor of 6 higher compared to the WE-CAN measurements
542 (GC-MS) but agreed within 60% with SEAC⁴RS (GC-MS) and FireLab EFs (PTR-MS). C₆H₈O (sum of 2,5-
543 dimethylfuran, 2-ethylfuran, and other C₂-substituted furan isomers), C₈H₁₀O₃ (syringol), and C₆H₄O₃ (hydroxy
544 benzoquinone) were quantified using estimated calibration factors during both campaigns, and therefore more
545 uncertain, and were higher by a factor of 2–5 during FIREX-AQ. Another influencing factor for the overall higher
546 EFs for oxygenated compounds during FIREX-AQ could be due to the optimized inlet setups to limit wall losses
547 prior to detection for the majority of the instruments (Table 2). Various oxygenated compounds are more analytically
548 sticky and can therefore partition to the inlet line walls prior to their detection. For example, during FIREX-AQ the
549 NOAA PTR-ToF-MS inlet line was 1-m long and heated at 60°C to reduce condensation sinks resulting in less than
550 1 second residence times; in Firelab (Koss et al., 2018) a longer 16 m transfer line was used at 40°C with a residence
551 time comparable to FIREX-AQ whereas in WE-CAN (Permar et al., 2021) the smoke to drift tube time was higher
552 (~ 2 seconds) at temperatures of 55–60°C. This could therefore contribute to differences for larger or more
553 oxygenated NMOGs between campaigns and partly explain the overall increased EFs during FIREX-AQ.

Deleted: methyl

556 Further differences between FIREX-AQ and WE-CAN may also result from the methods used to identify and
 557 characterize young plumes. As described in [Sect. 3.1](#), fresh plumes are identified during FIREX-AQ based on
 558 chemical aging proxies, whereas fresh plumes identified in WE-CAN are based on physical distance downwind. For
 559 highly reactive species, such as furans and oxygenated aromatics, strong fire-to-fire variability in OH exposure may
 560 alter emission factors, even in smoke with similar downwind age. Figure S2 compares the FIREX-AQ and WE-
 561 CAN field observations to the ERs obtained during the FireLab laboratory study for a variety of overlapping NMOGs
 562 with varying reactivities towards OH radicals. Given that FireLab experiments were performed under dark and
 563 warmer conditions in smoke aged just 5 seconds, it is expected that the more reactive compounds would show higher
 564 ERs when compared to field observations if the sampled smoke onboard the aircraft was already aged. However,
 565 higher ERs were observed for various compounds measured during FIREX-AQ. [In contrast](#), when comparing WE-
 566 CAN to FireLab ERs, the highly reactive compounds were lower although the ERs of less reactive compounds were
 567 in good agreement. This indicates possible differences between FIREX-AQ and WE-CAN owing to variability in
 568 chemical oxidation, which has the largest impact on highly reactive species.

569 The correlation to MCE for each species EFs was calculated for all wildfires as shown in Table S4 and compared to
 570 the WE-CAN observations. Correlation coefficients (R^2) during FIREX-AQ were above 0.5 for 28% of the species,
 571 0.3–0.5 for 27% of the species, and below 0.3 for the remaining species. The lowest correlations, below 0.1, were
 572 found for N-containing species, including particulate ammonium and pNO_x , ammonia, acetonitrile, 2-butyl nitrate,
 573 methyl nitrate, pyrrole and butene nitrile isomers, and acrylonitrile. Nevertheless, agreement within a factor of 2
 574 was found when compared to the slopes and R^2 obtained from the WE-CAN campaign for most of the compounds.
 575 Figure 6 shows the dependence of two N-containing species on fire MCEs for the FIREX-AQ and FireLab (Roberts
 576 et al., 2020) studies as well as for a majority of fuel types by Akagi et al. (2011) and Andreae (2019). We report N-
 577 containing species as a ratio to the total reactive nitrogen N_r , defined as the sum of NO , NO_2 , HONO, HCN, HCO,
 578 NH_3 , other N-containing VOCs, and particle-phase nitrate and ammonium. The dotted lines and shaded regions
 579 show FireLab parameterizations that describe how these ratios respond to changes in MCE (Roberts et al., 2020) for
 580 one [subalpine fir](#) fire burned during FireLab whereas square and bended square markers indicate different land cover
 581 types from Andreae (2019) and Akagi et al. (2011), respectively. It should be noted that for Akagi et al. (2011) and
 582 Andreae (2019) N_r measurements are limited to the sum of NO , NO_2 , HONO, HCN, and NH_3 and therefore the N_r
 583 could represent a lower limit. For both laboratory and field studies and independent of the fuel burnt, as MCE
 584 increases, NO_x/N_r increases, whereas NH_3/N_r decreases. The FireLab MCE ranged from pure flaming (MCE = 0.99)
 585 to smoldering values (MCE < 0.8), but ambient observations during FIREX-AQ were limited to MCE values ranging
 586 from 0.85 to 0.95, which suggests both flaming and smoldering contributions to the sampled wildfire plumes.



587
 588 **Figure 6:** Ratios of two N-species to the total nitrogen, N_r , during FIREX-AQ compared to Roberts et al. (2020) based on a
 589 [subalpine fir](#) fire burned during FireLab, and Andreae (2019) and Akagi et al. (2011) that include different land cover types.

Deleted: Section

Deleted: On

Deleted: the contrary

Deleted: one

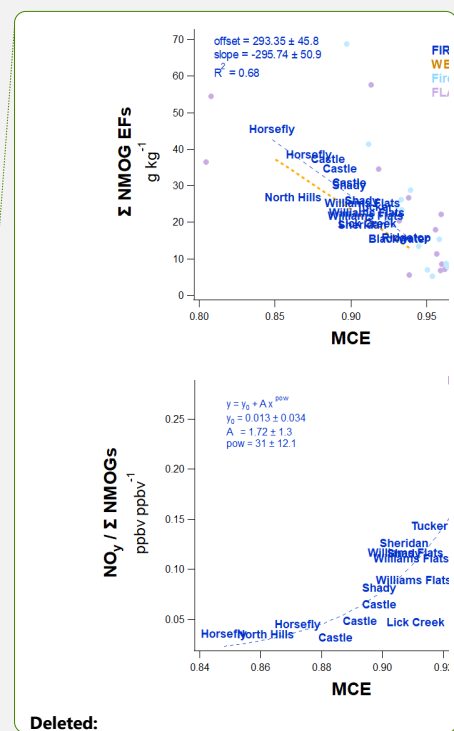
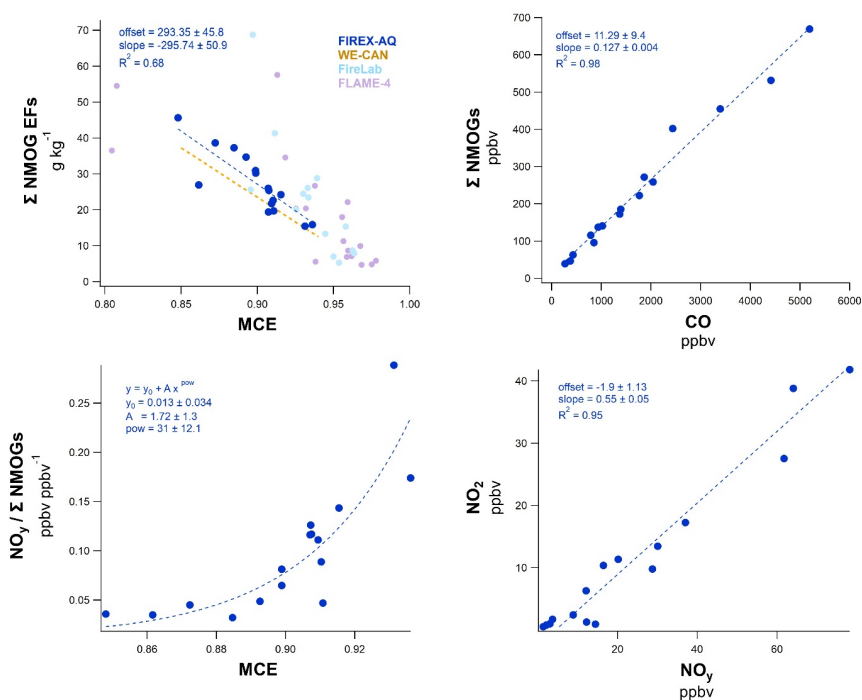
594 **3.5 Parameterization of organic- and nitrogen-containing emissions in wildfire plumes**

595 The comparisons described above demonstrate that FIREX-AQ emissions agreed within a factor of 2 or better with
596 previous laboratory and field studies for most C- and N-containing species for temperate ecosystem fuels. In the
597 following, we relate primary wildfire emissions and emission factors to fire emissions measurable from space, e.g.,
598 CO (e.g., Schneising et al., 2020), NO₂ (e.g., Martínez-Alonso et al., 2020), and BC (e.g., Konovalov et al., 2018),
599 as well as MCE. Although current satellite retrievals for wildfire smoke can agree with airborne observations e.g.,
600 for NO_x and CO (Griffin et al., 2021; Stockwell et al., 2022), challenges in isolating the fire contribution from small
601 or short-lived fires, as well as cloud coverage and aerosol interferences, add uncertainties to this quantification (e.g.,
602 Jung et al., 2019; Vasilkov et al., 2021). Here, we only focus on the parameterization of wildfire plumes and promote
603 future efforts to quantify these compounds using satellite retrievals more accurately. Satellite-retrieved
604 concentrations of CO and NO₂ close to wildfires could then be used to estimate NMOG and NO_y emissions and
605 potentially better account for variability associated with fire emissions and improve modeling efforts to simplify
606 and predict downwind formation of secondary pollutants, including ozone and secondary organic aerosol.

607 Figure 7 shows correlations between the sum of the median mixing ratios of NMOGs and NO_y with MCE, CO, and
608 NO₂, where CO and NO₂ are two species available from satellite products that could be used as proxies for
609 smoldering and flaming combustion (e.g., van der Velde et al., 2021; Urbanski et al., 2008), respectively. Figure 7a
610 shows that the sum of FIREX-AQ NMOG EFs correlated with MCE with an R² of 0.68, even though many of the
611 individual compounds are poorly correlated with MCE (Table S4). The correlation of the FIREX-AQ MCE to the
612 sum of NMOGs was in the same range as WE-CAN, FireLab, and FLAME-4 observations. WE-CAN was
613 consistently lower, by around 10%, which is partially due to differences in the assumed fraction of carbon employed
614 in Eq. (1) (45.7% for WE-CAN and 50% for this study). FIREX-AQ sampled fires with lower MCEs on average
615 than the lab experiments, with lab experiments showing highly variable EFs for MCE values below 0.9. Additional
616 reasons for different FireLab and FLAME-4 EFs vs. MCE are discussed in detail by Permar et al. (2021) and include,
617 (1) rapid chemistry prior to sampling, which results in the degradation of short-lived species (Fig. S2) and/or less
618 partitioning to particles at higher lab temperatures, (2) laboratory studies may more efficiently sample smoldering
619 combustion emissions compared to aircraft observations where residual smoldering combustion emissions might
620 not be lofted and therefore undersampled at the aircraft altitude, and (3) laboratory MCEs are often higher than in
621 the field due to experimental conditions, including drier fuel and more efficient burning conditions (Yokelson et al.,
622 2013; Holder et al., 2017; Selimovic et al., 2018), whereas field MCEs are calculated from single transects through
623 smoke plumes that likely contain a different mix of flaming vs. smoldering (Wiggins et al., 2020). Nevertheless, the
624 good agreement between two different aircraft studies during different years and the general agreement with FireLab
625 and FLAME-4 study averages further highlight the consistency of total NMOG correlations with MCE in wildfire
626 emissions despite the poorer correlations of individual compounds with MCE (Table S4).

Deleted:

Deleted: Figure



Deleted:

Deleted: Section

629

630 **Figure 7:** Correlation trends observed for western US wildfire emissions for (a) the sum of median NMOG EFs compared to
 631 MCE for each wildfire. Each data point represents one fire from either FIREX-AQ, WE-CAN (Permar et al., 2021), FireLab
 632 (Koss et al., 2018), or FLAME-4 (Stockwell et al., 2015) with the name of each FIREX-AQ fire centered on the data points. (b)
 633 Sum of median NMOG mixing ratios plotted vs. CO, (c) ratio of median NO_y species to the sum of NMOGs vs. MCE, and (d)
 634 median NO_y mixing ratios vs. the median NO₂ concentration. Dashed lines indicate linear fits for (a), (b), and (d), and a power
 635 function fit for (c).

636 Figure 7b relates the sum of the median NMOG mixing ratios to the median CO mixing ratios for all the freshest
 637 sampled wildfire plumes. CO results largely from smoldering combustion, which is the combustion process that also
 638 produces most NMOGs. NMOGs and CO are very well correlated, with a slope of 127 ± 4 (ppb ppm⁻¹) and an R²
 639 of 0.98, which demonstrates that total primary NMOG emissions are effectively represented by CO. Figure S4 shows
 640 that R² values with CO for individual compounds were above 0.9 for the majority of primary NMOGs reported here,
 641 whereas, for secondary species, the correlations were below 0.3. CO columns are retrievable from space by, e.g.,
 642 TROPOMI (Martínez-Alonso et al., 2020) and CRiS (NASA, 2015) and can be used to derive CO emissions that
 643 generally agree with *in situ* observations (Stockwell et al., 2022). The correlations from the FIREX-AQ
 644 measurements and others could be used to initialize total NMOG emissions from wildfire plumes in models.

645 Quantification of N-containing species is also essential for understanding and modeling the evolution and formation
 646 of secondary organic aerosol and ozone downwind of wildfires. Figure 7c shows the ratio of measured NO_y by the
 647 chemiluminescence instrument (see Sect. 2.1), to the sum of NMOGs in ppb ppb⁻¹. A rapid increase in this ratio is
 648 observed as MCE increases described by a power function fit. This increase follows the expectation that as fires
 649 transition from smoldering to flaming conditions, MCE increases, NMOGs EFs decrease, and fuel nitrogen leads to
 650 the formation of NO_x through radical chemistry of N-containing compounds (Roberts et al., 2020). Figure 7d shows
 651 that NO₂ represents a significant fraction of NO_y with a slope of 0.55 ± 0.03 (ppb ppb⁻¹) and an R² of 0.95.
 652 Furthermore, the correlation of individual N-containing species with NO₂ is significantly higher than their

655 correlation with CO mixing ratios (Fig. S4) promoting that NO₂ measurements could be used to initialize total NO_y
 656 emissions and N-species from wildfire plumes in models. Figure S5 shows additional correlations that could be used
 657 for modeling efforts, including the correlation of NO_y to CO, NO_y to BC, and others.

Deleted: Figure

Deleted: s

658 These observations suggest that CO is a good proxy for species emitted from western wildfires primarily during
 659 smoldering conditions (i.e., NMOGs), whereas NO₂ is a good proxy for species that are mostly emitted during
 660 flaming conditions (i.e., mostly NO_y). Thus, in addition to coupling EFs with fuel consumption to derive emissions,
 661 we suggest future use of satellite retrievals close to the fire plume to quantify CO and NO₂ concentrations in order
 662 to accurately determine EFs for all carbon and nitrogen-containing species for western US wildfire plumes as input
 663 to models. An important assumption, especially in determining emissions of N-containing species, is that NO₂
 664 should accurately represent NO_y close to the fire. However, satellite retrievals that capture truly fresh emissions very
 665 close to the fire will be dominated by NO and HONO whereas in highly oxidized plumes NO₂ loss processes will
 666 lower its overall contribution to NO_y. It is therefore important to provide a range of distances where this holds true.
 667 Coggon et al. (2022) find that for fires with highly reactive emissions, NO₂ represents NO_y within the first 15-30
 668 min and a distance of 10-20 km downwind of the fire assuming a wind speed 10 m/s. Current satellite retrievals for
 669 wildfire smoke have a spatial resolution of 3.5 km × 5.5 km (Griffin et al., 2021) which would be within the above
 670 range and high enough to represent plumes where NO₂ is the dominant fraction of NO_y.

671 **Table 3:** Emission ratios and emission factors of organic and nitrogen compounds from wildfire plumes. In blue are multiple
 672 isomers measured as a sum by the NOAA PTR-ToF-MS that were further speciated based on other GC-MS measurements from
 673 FIREX-AQ (column 1 in parentheses). Here, we show the ratio of each isomer measured by GC-MS to the total PTR-ToF-MS
 674 signal obtained in this mass.

Deleted: parenthesis

Compound <i>Isomer contribution to each mass is provided in parentheses based on the ratio of each isomer measured by GC-MS to the sum measured by PTR-ToF-MS (check Table S5)</i>	Instrument	Exact Mass, Da	Chemical formula/structure	EFs (g kg ⁻¹)	± σ	ERs to CO (ppb ppm ⁻¹)	± σ
Gas-Phase							
Carbon dioxide	DACOM	43.99	CO ₂	1533.82	78.06	9400.32	2455.30
Carbon monoxide	DACOM	27.99	CO	109.15	22.70	1000.00	0.00
Methane	DACOM	16.03	CH ₄	5.81	2.68	91.97	31.61
Formaldehyde	CAMS & ISAF	30.01	CH ₂ O	2.10	0.79	17.92	4.31
Acetic acid + Glycolaldehyde	NOAA PTR-ToF-MS for the sum	60.02	C ₂ H ₄ O ₂	2.09	0.61	8.86	1.51
Acetaldehyde	NOAA PTR-ToF-MS	44.03	C ₂ H ₄ O	1.95	0.60	11.25	1.70
Ethene	iWAS	28.03	C ₂ H ₄	1.52	0.45	13.57	1.97
Methanol	NOAA PTR-ToF-MS	32.03	CH ₄ O	1.42	0.66	10.90	3.21
5-Methylfurfural + Benzene diols (=Catechol, Resorcinol)	NOAA PTR-ToF-MS for the sum	110.11	C ₆ H ₆ O ₂	1.20	0.47	2.72	0.68
Acetone (78%) + Propanal (22%)	NOAA PTR-ToF-MS (speciation by GC-MS)	58.04	C ₃ H ₆ O	0.93	0.34	4.04	0.84
Ethane	iWAS	30.05	C ₂ H ₆	0.91	0.26	7.76	1.84
Methyl acetate + Ethyl formate + Hydroxyacetone	NOAA PTR-ToF-MS for the sum	74.04	C ₃ H ₆ O ₂	0.81	0.36	2.70	0.73
Propene	iWAS	42.05	C ₃ H ₆	0.80	0.27	4.80	1.16
MVK (38%) + Methacrolein (27%) + 2-Butenal (33%)	NOAA PTR-ToF-MS (speciation by GC-MS)	70.09	C ₄ H ₆ O	0.71	0.27	2.56	0.56

Deleted: parenthesis

Benzene	NOAA PTR-ToF-MS	78.05	C6H6	0.69	0.17	2.26	0.24
Guaiacol (=2-Methoxyphenol)	NOAA PTR-ToF-MS	124.14	C7H8O2	0.70	0.34	1.38	0.52
Acrolein	NOAA PTR-ToF-MS	56.03	C3H4O	0.88	0.88	3.73	2.73
Methyl glyoxal	ACES	72.06	CH3COCHO	0.44	0.36	1.55	1.23
Isocyanic acid	NOAA PTR-ToF-MS	43.01	HNCO	0.53	0.31	3.51	2.46
Formic acid	NOAA PTR-ToF-MS	46.00	HCOOH	0.60	0.43	3.31	1.95
2-Methylphenol (=o-cresol) + Anisol	NOAA PTR-ToF-MS for the sum	108.14	C7H8O	0.57	0.22	1.32	0.37
2(3H)-Furanone	NOAA PTR-ToF-MS	84.02	C4H4O2	0.54	0.26	1.60	0.50
HCN	CIT-CIMS	27.01	HCN	0.31	0.12	3.01	1.08
Toluene	NOAA PTR-ToF-MS	92.06	C7H8	0.53	0.21	1.42	0.35
2,3-Butanedione + 2-Oxobutanal + 1,4-Butanedial	NOAA PTR-ToF-MS for the sum	86.04	C4H6O2	0.49	0.20	1.43	0.37
Monoterpenes	NOAA PTR-ToF-MS	136.24	C10H16	0.47	0.43	0.82	0.65
2-Methoxy-4-methylphenol (= Creosol)	NOAA PTR-ToF-MS	138.16	C8H10O2	0.47	0.26	0.82	0.36
2,5-Dimethylfuran + 2-Ethylfuran + Other unidentified organic compounds	NOAA PTR-ToF-MS for the sum	96.06	C6H8O	0.41	0.16	1.07	0.27
Phenol	CIT-CIMS	94.04	C6H6O	0.16	0.05	0.43	0.13
Furan	TOGA	68.03	C4H4O	0.35	0.13	1.33	0.40
i-Butene	iWAS	56.06	C4H8	0.35	0.12	1.61	0.42
Acetonitrile	NOAA PTR-ToF-MS	41.03	C2H3N	0.32	0.14	2.04	0.86
Propane	iWAS	44.06	C3H8	0.33	0.14	1.90	0.66
Ethyne	iWAS	26.02	C2H2	0.30	0.14	2.90	0.92
Glyoxal	ACES	58.04	CHOCHO	0.22	0.20	0.94	0.78
MEK	NOAA PTR-ToF-MS	72.06	C4H8O	0.24	0.08	0.84	0.20
Ethylbenzene (7%) + m- and p-Xylenes (58%) + o-Xylene (21%)	NOAA PTR-ToF-MS (speciation by GC-MS)	106.17	C8H10	0.08	0.04	0.18	0.07
2-Furfural	TOGA	96.02	C5H4O2	0.18	0.06	0.47	0.11
Benzaldehyde	NOAA PTR-ToF-MS	106.12	C7H6O	0.15	0.05	0.35	0.06
1-Butene	iWAS	56.06	C4H8	0.15	0.05	0.68	0.16
Hydroxy benzoquinone	NOAA PTR-ToF-MS	124.09	C6H4O3	0.12	0.06	0.23	0.09
2-Methylfuran	TOGA	82.04	C5H6O	0.11	0.04	0.34	0.10
Styrene	NOAA PTR-ToF-MS	104.15	C8H8	0.11	0.04	0.26	0.06
C9 Aromatics	NOAA PTR-ToF-MS	120.19	C9H12	0.084	0.043	0.178	0.073
Naphthalene	NOAA PTR-ToF-MS	128.17	C10H8	0.077	0.032	0.161	0.074
n-Butane	iWAS	58.08	C4H10	0.082	0.030	0.368	0.121
Benzonitrile	NOAA PTR-ToF-MS	103.04	C7H5N	0.081	0.027	0.200	0.062
1-Pentene	iWAS	70.08	C5H10	0.073	0.023	0.268	0.069
Benzofuran	NOAA PTR-ToF-MS	118.10	C8H6O	0.067	0.023	0.143	0.031
Butanal	TOGA	72.06	C4H8O	0.060	0.019	0.217	0.064
Isoprene	iWAS	68.06	C5H8	0.070	0.055	0.271	0.203
Propyne	WAS	40.03	C3H4	0.057	0.027	0.362	0.121
2-Methyl-1-butene	iWAS	70.08	C5H10	0.055	0.020	0.201	0.054
Nitromethane	NOAA PTR-ToF-MS	61.02	CH3NO2	0.052	0.025	0.228	0.116
1-Hexene	WAS	84.09	C6H12	0.049	0.013	0.151	0.043
2-Methylpropanal	TOGA	72.06	C4H8O	0.046	0.015	0.167	0.049

Deleted: -

n-Pentane	iWAS	72.09	C5H12	0.044	0.018	0.159	0.058
Acrylonitrile	NOAA PTR-ToF-MS	53.03	C3H3N	0.040	0.011	0.202	0.073
cis-2-Butene	iWAS	56.06	C4H8	0.013	0.005	0.045	0.013
Syringol	NOAA PTR-ToF-MS	154.17	C8H10O3	0.047	0.034	0.078	0.056
trans-1,3-Pentadiene	iWAS	68.06	C5H8	0.033	0.015	0.123	0.044
trans-2-Butene	iWAS	56.06	C4H8	0.037	0.020	0.166	0.082
n-Hexane	iWAS	86.11	C6H14	0.033	0.013	0.099	0.038
i-Butane	iWAS	58.08	C4H10	0.027	0.010	0.122	0.038
1-Heptene	WAS	98.11	C7H14	0.026	0.008	0.069	0.022
Ethanol	NOAA PTR-ToF-MS	46.04	C2H6O	0.020	0.055	0.098	0.273
n-Nonane	iWAS	128.16	C9H20	0.025	0.010	0.051	0.020
Methyl formate	iWAS	60.02	C2H4O2	0.020	0.022	0.089	0.095
n-Decane	iWAS	142.17	C10H22	0.023	0.012	0.042	0.024
3-Methylfuran	TOGA	82.04	C5H6O	0.019	0.006	0.058	0.017
1-Octene	WAS	112.13	C8H16	0.018	0.005	0.042	0.013
3-Furfural	TOGA	96.02	C5H4O2	0.018	0.006	0.047	0.011
trans-2-Pentene	iWAS	70.08	C5H10	0.018	0.008	0.065	0.025
2,4-Dimethylpentane	iWAS	100.13	C7H16	0.018	0.009	0.046	0.019
1-Nonene	WAS	126.14	C9H18	0.015	0.005	0.031	0.011
1-Buten-3-yne	WAS	52.03	C4H4	0.014	0.007	0.070	0.026
Pyrrrole	TOGA	67.04	C4H5N	0.012	0.005	0.047	0.024
i-Pentane	iWAS	72.09	C5H12	0.012	0.006	0.045	0.023
cis-2-Pentene	iWAS	70.08	C5H10	0.013	0.005	0.045	0.013
Butene nitrile isomers	TOGA	67.04	C4H5N	0.007	0.003	0.028	0.014
2-Methylpentane	iWAS	86.11	C6H14	0.007	0.003	0.020	0.008
1-Butyne	WAS	54.05	C4H6	0.006	0.003	0.030	0.012
Methylcyclopentane	iWAS	84.09	C6H12	0.005	0.002	0.015	0.006
Methylcyclohexane	iWAS	98.11	C7H14	0.004	0.002	0.011	0.006
Dimethyl sulfide (50%) + other unidentified organic compounds (50%)	NOAA PTR-ToF-MS (speciation by GC-MS)	62.02	C2H6S	0.002	0.002	0.009	0.007
2-Butyne	WAS	54.05	C4H6	0.003	0.002	0.014	0.008
Methyl nitrate	WAS	77.01	CH3NO3	0.002	0.002	0.008	0.005
i-Propanol	WAS	60.06	C3H8O	0.003	0.006	0.015	0.026
i-Propyl nitrate	WAS	105.04	C3H7NO3	0.002	0.001	0.005	0.002
1,3-Butadiyne	WAS	50.02	C4H2	0.001	0.001	0.006	0.002
Ethyl nitrate	WAS	91.03	C2H5NO3	0.001	0.001	0.002	0.002
2-Butyl nitrate	WAS	119.06	C4H9NO3	0.0005	0.001	0.001	0.002
NO _y	CL		NO _y			12.10	7.38
Nitrogen dioxide	CL	46.01	NO ₂	0.93	0.63	6.05	5.34
Nitric oxide	CL	30.01	NO	0.14	0.13	1.42	1.44
Nitrous acid	NOAA CIMS	47.00	HONO	0.30	0.21	1.89	1.61
Ammonia	Oslo PTR-ToF-MS	17.03	NH ₃	1.15	0.77	17.44	11.65

Deleted: Cis

Deleted: 2-Methyl-1-Butene

Deleted: iWAS

Deleted: 70.08

Deleted: C5H10

Deleted: 0.055

Deleted: 0.020

Deleted: 0.201

Deleted: 0.054

Deleted: Pentadiene

Deleted: Trans

Deleted: F

Deleted: Trans

Deleted: cis-2-Butene

Deleted: N

Deleted: i

Deleted: i

Deleted: i

Deleted: i

Deleted: i

Deleted: 1.

Deleted: 1

Deleted: 22

Deleted: 6

Deleted: 16

Aerosol-Phase (all units in g/kg)

Organic aerosol (OA/OC = 1.89 ± 0.16)	AMS		OA	26.51	13.97	317.3	148.9
Particulate nitrate	AMS	62.00	pNO _y	0.84	0.3	7.29	2.69
Particulate ammonium	AMS	18.04	pNH ₄ ⁺	0.36	0.21	3.24	1.97
Black carbon	SP2		BC	0.35	0.32	3.26	2.69
Sums							
NH _x as NH ₃ (EF _{NH3} + (17/18)* EF _{NH4})	UIBK/UIO PTR- ToF-MS + AMS	17.03	NH ₃	1.65	1.14	24.56	17.10
NO _x as NO (EF _{NO} + (30/46)* EF _{NO2})	CL	30.01	NO	0.87	0.96	5.37	4.92
SO _x as SO ₂	NO-LIF, AMS		See <i>Rickly et al. (2022)</i>				
Total NMOGs emissions				26.88	8.5	134.24	18.23

Deleted: 85

Deleted: 1.19

Deleted: 78

Deleted: 5

Deleted: 37

Deleted: 23.80

Deleted: 7

Deleted: 135.02

Conclusions

We present ERs and EFs for NMOGs and nitrogen-containing compounds from nine western US wildfires and one southeastern US prescribed fire derived from data obtained aboard the NASA DC-8 during the 2019 FIREX-AQ mission. ERs and EFs were calculated for a total of 16 crosswind plume transects chosen to represent the freshest fire emissions. These transects were identified based on proxies (e.g., maleic anhydride/furan ratio) for chemical aging, which can be rapid in fire plumes.

We performed detailed comparisons of FIREX-AQ emissions to previous laboratory and field studies with a focus on oxygenated organic compounds that were calibrated during this mission. FIREX-AQ ERs agree within a factor of 2 to the FireLab study for most compounds, with a correlation slope of 0.75 ± 0.05 and an R^2 of 0.86. A comparison of the field-derived EFs from FIREX-AQ with those from SEAC⁴RS (Liu et al., 2017), WE-CAN (Permar et al., 2021), and temperate forest EFs from Andreae (2019) also agreed to within a factor of 2 for 87%, 83%, and 78% of the compounds, respectively. However, FIREX-AQ EFs are on average higher compared to previous studies. For compounds that agree within a factor of 2, the average ratios of FIREX-AQ to WE-CAN, SEAC⁴RS, and the temperate forest fire literature average are 1.09 ± 0.3 , 1.25 ± 0.33 , and 1.18 ± 0.4 , respectively, whereas for the remaining compounds, the ratios increase to 2.1 ± 1.64 , 1.29 ± 1.01 , and 1.32 ± 1.23 . We suggest that these differences could be due to differences in the fuel, quantification methods applied for each study, as well as due to differences in photochemical loss of reactive species prior to detection. Additionally, differences in fire behavior and the lofting of smoke, including variations in the mixture of flaming and smoldering combustion, could also be contributing factors. We further compare the ratio of N-containing species to the total nitrogen (N_i/N_t) vs. MCE and find that NO_x/N_t and NH_3/N_t follow similar trends as those reported by Roberts et al. (2020).

Deleted: R

We relate wildfire emissions of C- and N-containing species to CO, NO₂, BC, and MCE based on correlations for use in chemical transport models. Results show that the sum of NMOG EFs correlates with MCE, with an R^2 of 0.68 and a slope of -296 ± 51 g kg⁻¹. A better correlation is observed between the sum of the median NMOG mixing ratios and median CO, with a slope of 0.127 ± 0.004 (ppb ppm⁻¹) and an R^2 of 0.98. Consistent correlation of individual NMOGs to CO is also evident for the majority of NMOGs with R^2 values greater than 0.9, suggesting significant potential for estimating wildfire NMOG emissions using space-based CO emissions.

For N-containing species, the sum of reactive nitrogen, NO_y, correlates better with NO₂ ($R^2 = 0.95$, slope = 1.74 ± 0.1 ppbv ppbv⁻¹) and BC ($R^2 = 0.88$) than with CO ($R^2 = 0.7$) close to wildfires. Furthermore, the ratio of NO_y to the sum of NMOGs increases exponentially as MCE increases. This further highlights the important influence of fire behavior, e.g., flaming vs. smoldering fire conditions on the emissions of reactive nitrogen species. Future efforts to initialize models using the above emissions parameterization could improve the representation of fire emissions in

Deleted: the

747 models and their predictions on the downwind formation of secondary pollutants like ozone and secondary organic
748 aerosol.

749 Acknowledgments

750 We would like to thank the NOAA/NASA FIREX-AQ science and aircraft operation teams. GIG, MMC, CES, MMB, IB,
751 JMK, AL, SAM, JAN, JP, PSR, MAR, RHS, CCW, and CW were supported by the NOAA Cooperative Agreement with
752 CIRES, NA17OAR4320101. RY and VS acknowledge NOAA grant NA16OAR4310100 and NSF grant 1748266. JL,
753 GMW, RAH, JMS, and TFH acknowledge support from the NASA Tropospheric Composition Program and NOAA
754 Climate Program Office's Atmospheric Chemistry, Carbon Cycle and Climate (AC4) program (NA17OAR4310004). DP,
755 BAN, HG, PCJ, DAD, MKS, and JLJ were supported by NASA grants 80NSSC18K0630 and 80NSSC21K1451. AF was
756 supported by NASA TCP Grant No. 80NSSC18K0628. The University of Innsbruck team was supported by the Austrian
757 Federal Ministry for Transport, Innovation, and Technology (bmvit, FFG, ASAP). FP received funding from the European
758 Union's Horizon 2020 research and innovation program under grant agreement No. 674911 (IMPACT EU ITN). LX, KTV,
759 HA, JDC, and POW acknowledge NASA grant 80NSSC18K0660 and 80NSSC21K1704. This material is based upon work
760 supported by the National Center for Atmospheric Research, sponsored by the National Science Foundation under
761 Cooperative Agreement No. 1852977.

762

763 References

- 764 Akagi, S. K., Yokelson, R. J., Wiedinmyer, C., Alvarado, M. J., Reid, J. S., Karl, T., Crounse, J. D., and Wennberg, P.
765 O.: Emission factors for open and domestic biomass burning for use in atmospheric models, *Atmos. Chem. Phys.*, 11,
766 4039-4072, <https://doi.org/10.5194/acp-11-4039-2011>, 2011.
- 767 Akagi, S. K., Craven, J. S., Taylor, J. W., McMeeking, G. R., Yokelson, R. J., Burling, I. R., Urbanski, S. P., Wold, C.
768 E., Seinfeld, J. H., Coe, H., Alvarado, M. J., and Weise, D. R.: Evolution of trace gases and particles emitted by a
769 chaparral fire in California, *Atmos. Chem. Phys.*, 12, 1397-1421, <https://doi.org/10.5194/acp-12-1397-2012>, 2012.
- 770 Akagi, S. K., Burling, I. R., Mendoza, A., Johnson, T. J., Cameron, M., Griffith, D. W. T., Paton-Walsh, C., Weise, D.
771 R., Reardon, J., and Yokelson, R. J.: Field measurements of trace gases emitted by prescribed fires in southeastern US
772 pine forests using an open-path FTIR system, *Atmos. Chem. Phys.*, 14, 199-215, [https://doi.org/10.5194/acp-14-199-](https://doi.org/10.5194/acp-14-199-2014)
773 [2014](https://doi.org/10.5194/acp-14-199-2014), 2014.
- 774 Andreae, M. O. and Merlet, P.: Emission of trace gases and aerosols from biomass burning, *Global Biogeochem. Cy.*, 15,
775 955-966, <https://doi.org/10.1029/2000GB001382>, 2001.
- 776 Andreae, M. O.: Emission of trace gases and aerosols from biomass burning – an updated assessment, *Atmos. Chem.*
777 *Phys.*, 19, 8523-8546, <https://doi.org/10.5194/acp-19-8523-2019>, 2019.
- 778 Apel, E. C., Emmons, L. K., Karl, T., Flocke, F., Hills, A. J., Madronich, S., Lee-Taylor, J., Fried, A., Weibring, P.,
779 Walega, J., Richter, D., Tie, X., Mauldin, L., Campos, T., Weinheimer, A., Knapp, D., Sive, B., Kleinman, L.,
780 Springston, S., Zaveri, R., Ortega, J., Voss, P., Blake, D., Baker, A., Warneke, C., Welsh-Bon, D., de Gouw, J., Zheng,
781 J., Zhang, R., Rudolph, J., Junkermann, W., and Riemer, D. D.: Chemical evolution of volatile organic compounds in the
782 outflow of the Mexico City Metropolitan area, *Atmos. Chem. Phys.*, 10, 2353-2375, [https://doi.org/10.5194/acp-10-](https://doi.org/10.5194/acp-10-2353-2010)
783 [2353-2010](https://doi.org/10.5194/acp-10-2353-2010), 2010.
- 784 Apel, E. C., Hornbrook, R. S., Hills, A. J., Blake, N. J., Barth, M. C., Weinheimer, A., Cantrell, C., Rutledge, S. A.,
785 Basarab, B., Crawford, J., Diskin, G., Homeyer, C. R., Campos, T., Flocke, F., Fried, A., Blake, D. R., Brune, W.,
786 Pollack, I., Peischl, J., Ryerson, T., Wennberg, P. O., Crounse, J. D., Wisthaler, A., Mikoviny, T., Huey, G., Heikes, B.,
787 O'Sullivan, D., and Riemer, D. D.: Upper tropospheric ozone production from lightning NO_x-impacted convection:
788 Smoke ingestion case study from the DC3 campaign, *J. Geophys. Res. Atmos.*, 120, 2505-2523,
789 <https://doi.org/10.1002/2014JD022121>, 2015.
- 790 Apte, J. S., Brauer, M., Cohen, A. J., Ezzati, M., and Pope, C. A.: Ambient PM_{2.5} Reduces Global and Regional Life
791 Expectancy, *Environ. Sci. Tech. Lett.*, 5, 546-551, <https://doi.org/10.1021/acs.estlett.8b00360>, 2018.
- 792
793
794
795
796
797
798
799

800 Bond, T. C., Doherty, S. J., Fahey, D. W., Forster, P. M., Berntsen, T., DeAngelo, B. J., Flanner, M. G., Ghan, S.,
801 Kärcher, B., Koch, D., Kinne, S., Kondo, Y., Quinn, P. K., Sarofim, M. C., Schultz, M. G., Schulz, M., Venkataraman,
802 C., Zhang, H., Zhang, S., Bellouin, N., Guttikunda, S. K., Hopke, P. K., Jacobson, M. Z., Kaiser, J. W., Klimont, Z.,
803 Lohmann, U., Schwarz, J. P., Shindell, D., Storelvmo, T., Warren, S. G., and Zender, C. S.: Bounding the role of black
804 carbon in the climate system: A scientific assessment, *J. Geophys. Res. Atmos.*, 118, 5380-5552,
805 <https://doi.org/10.1002/jgrd.50171>, 2013.

806
807 Balch, J. K., Bradley, B. A., Abatzoglou, J. T., Nagy, R. C., Fusco, E. J., and Mahood, A. L.: Human-started wildfires
808 expand the fire niche across the United States, *P. Natl. Acad. Sci. USA*, 114, 2946,
809 <https://doi.org/10.1073/pnas.1617394114>, 2017.

810
811 Bourgeois, I., Peischl, J., Thompson, C. R., Aikin, K. C., Campos, T., Clark, H., Commane, R., Daube, B., Diskin, G.
812 W., Elkins, J. W., Gao, R. S., Gaudel, A., Hints, E. J., Johnson, B. J., Kivi, R., McKain, K., Moore, F. L., Parrish, D. D.,
813 Querel, R., Ray, E., Sánchez, R., Sweeney, C., Tarasick, D. W., Thompson, A. M., Thouret, V., Witte, J. C., Wofsy, S.
814 C., and Ryerson, T. B.: Global-scale distribution of ozone in the remote troposphere from the ATom and HIPPO airborne
815 field missions, *Atmos. Chem. Phys.*, 20, 10611-10635, <https://doi.org/10.5194/acp-20-10611-2020>, 2020.

816
817 Bourgeois, I., Peischl, J., Neuman, J. A., Brown, S. S., Allen, H. M., Campuzano-Jost, P., Coggon, M. M., DiGangi, J.
818 P., Diskin, G. S., Gilman, J. B., Gkatzelis, G. I., Guo, H., Halliday, H. A., Hanisco, T. F., Holmes, C. D., Huey, L. G.,
819 Jimenez, J. L., Lamplugh, A. D., Lee, Y. R., Lindaas, J., Moore, R. H., Nault, B. A., Nowak, J. B., Pagonis, D., Rickly,
820 P. S., Robinson, M. A., Rollins, A. W., Selimovic, V., St. Clair, J. M., Tanner, D., Vasquez, K. T., Veres, P. R.,
821 Warneke, C., Wennberg, P. O., Washenfelder, R. A., Wiggins, E. B., Womack, C. C., Xu, L., Zarzana, K. J., and
822 Ryerson, T. B.: Comparison of airborne measurements of NO, NO₂, HONO, NO_y, and CO during FIREX-AQ, *Atmos.*
823 *Meas. Tech.*, 15, 4901-4930, <https://doi.org/10.5194/amt-15-4901-2022>, 2022.

824
825 Braga, R. C., Rosenfeld, D., Weigel, R., Jurkat, T., Andreae, M. O., Wendisch, M., Pöschl, U., Voigt, C., Mahnke, C.,
826 Borrmann, S., Albrecht, R. I., Molleker, S., Vila, D. A., Machado, L. A. T., and Grulich, L.: Further evidence for CCN
827 aerosol concentrations determining the height of warm rain and ice initiation in convective clouds over the Amazon
828 basin, *Atmos. Chem. Phys.*, 17, 14433-14456, <https://doi.org/10.5194/acp-17-14433-2017>, 2017.

829
830 Brey, S. J. and Fischer, E. V.: Smoke in the City: How Often and Where Does Smoke Impact Summertime Ozone in the
831 United States? *Environ. Sci. Technol.*, 50, <https://doi.org/10.1021/acs.est.5b05218>, 2015.

832
833 Canagaratna, M. R., Jayne, J. T., Jimenez, J. L., Allan, J. D., Alfarra, M. R., Zhang, Q., Onasch, T. B., Drewnick, F.,
834 Coe, H., Middlebrook, A., Delia, A., Williams, L. R., Trimborn, A. M., Northway, M. J., DeCarlo, P. F., Kolb, C. E.,
835 Davidovits, P., and Worsnop, D. R.: Chemical and microphysical characterization of ambient aerosols with the aerodyne
836 aerosol mass spectrometer, *Mass Spectrom. Rev.*, 26, 185-222, <https://doi.org/10.1002/mas.20115>, 2007.

837
838 Cazorla, M., Wolfe, G. M., Bailey, S. A., Swanson, A. K., Arkinson, H. L., and Hanisco, T. F.: A new airborne laser-
839 induced fluorescence instrument for in situ detection of formaldehyde throughout the troposphere and lower stratosphere,
840 *Atmos. Meas. Tech.*, 8, 541-552, <https://doi.org/10.5194/amt-8-541-2015>, 2015.

841
842 Cecchini, M. A., Machado, L. A. T., Andreae, M. O., Martin, S. T., Albrecht, R. I., Artaxo, P., Barbosa, H. M. J.,
843 Borrmann, S., Fütterer, D., Jurkat, T., Mahnke, C., Minikin, A., Molleker, S., Pöhlker, M. L., Pöschl, U., Rosenfeld, D.,
844 Voigt, C., Weinzierl, B., and Wendisch, M.: Sensitivities of Amazonian clouds to aerosols and updraft speed, *Atmos.*
845 *Chem. Phys.*, 17, <https://doi.org/10.5194/acp-17-10037-2017>, 2017.

846
847 Cochrane, M. A., Moran, C. J., Wimberly, M. C., Baer, A. D., Finney, M. A., Beckendorf, K. L., Eidenshink, J., and
848 Zhu, Z.: Estimation of wildfire size and risk changes due to fuels treatments, *Int. J. Wildland Fire*, 21, 357-367,
849 <https://doi.org/10.1071/WF11079>, 2012.

850
851 Coggon, M. M., Lim, C. Y., Koss, A. R., Sekimoto, K., Yuan, B., Gilman, J. B., Hagan, D. H., Selimovic, V., Zarzana,
852 K. J., Brown, S. S., Roberts, J. M., Müller, M., Yokelson, R., Wisthaler, A., Krechmer, J. E., Jimenez, J. L., Cappa, C.,
853 Kroll, J. H., de Gouw, J., and Warneke, C.: OH chemistry of non-methane organic gases (NMOGs) emitted from
854 laboratory and ambient biomass burning smoke: evaluating the influence of furans and oxygenated aromatics on ozone
855 and secondary NMOG formation, *Atmos. Chem. Phys.*, 19, 14875-14899, <https://doi.org/10.5194/acp-19-14875-2019>,
856 2019.

857
858 Colman, J. J., Swanson, A. L., Meinardi, S., Sive, B. C., Blake, D. R., and Rowland, F. S.: Description of the Analysis of
859 a Wide Range of Volatile Organic Compounds in Whole Air Samples Collected during PEM-Tropics A and B, *Anal.*
860 *Chem.*, 73, 3723-3731, <https://doi.org/10.1021/ac010027g>, 2001.

861
862
863
864
865
866
867
868
869
870
871
872
873
874
875
876
877
878
879
880
881
882
883
884
885
886
887
888
889
890
891
892
893
894
895
896
897
898
899
900
901
902
903
904
905
906
907
908
909
910
911
912
913
914
915
916
917
918
919
920
921

Crouse, J. D., McKinney, K. A., Kwan, A. J., and Wennberg, P. O.: Measurement of Gas-Phase Hydroperoxides by Chemical Ionization Mass Spectrometry, *Anal. Chem.*, 78, 6726-6732, <https://doi.org/10.1021/ac0604235>, 2006.

Crutzen, P. J. and Andreae, M. O.: Biomass Burning in the Tropics: Impact on Atmospheric Chemistry and Biogeochemical Cycles, *Science*, 250, 1669, <https://doi.org/10.1126/science.250.4988.1669>, 1990.

Day, D. A., Campuzano-Jost, P., Nault, B. A., Palm, B. B., Hu, W., Guo, H., Wooldridge, P. J., Cohen, R. C., Docherty, K. S., Huffman, J. A., de Sá, S. S., Martin, S. T., and Jimenez, J. L.: A Systematic Re-evaluation of Methods for Quantification of Bulk Particle-phase Organic Nitrates Using Real-time Aerosol Mass Spectrometry, *Atmos. Meas. Tech.*, 15, 459-483, <https://doi.org/10.5194/amt-15-459-2022>, 2022.

Decker, Z. C. J., Robinson, M. A., Barsanti, K. C., Bourgeois, I., Coggon, M. M., DiGangi, J. P., Diskin, G. S., Flocke, F. M., Franchin, A., Fredrickson, C. D., Hall, S. R., Halliday, H., Holmes, C. D., Huey, L. G., Lee, Y. R., Lindsaas, J., Middlebrook, A. M., Montzka, D. D., Moore, R. H., Neuman, J. A., Nowak, J. B., Palm, B. B., Peischl, J., Piel, F., Rickly, P. S., Rollins, A. W., Ryerson, T. B., Schwantes, R. H., Sekimoto, K., Thornhill, L., Thornton, J. A., Tyndall, G. S., Ullmann, K., Van Rooy, P., Veres, P. R., Warneke, C., Washenfelder, R. A., Weinheimer, A. J., Wiggins, E., Winstead, E., Wisthaler, A., Womack, C., and Brown, S. S.: Nighttime and daytime dark oxidation chemistry in wildfire plumes: an observation and model analysis of FIREX-AQ aircraft data, *Atmos. Chem. Phys.*, 21, 16293-16317, <https://doi.org/10.5194/acp-21-16293-2021>, 2021.

Dennekamp, M., Straney, L. D., Erbas, B., Abramson, M. J., Keywood, M., Smith, K., Sim, M. R., Glass, D. C., Del Monaco, A., Haikerwal, A., and Tonkin, A. M.: Forest Fire Smoke Exposures and Out-of-Hospital Cardiac Arrests in Melbourne, Australia: A Case-Crossover Study, *Environ. Health Persp.*, 123, 959-964, <https://doi.org/10.1289/ehp.1408436>, 2015.

Finewax, Z., de Gouw, J. A., and Ziemann, P. J.: Identification and Quantification of 4-Nitrocatechol Formed from OH and NO₃ Radical-Initiated Reactions of Catechol in Air in the Presence of NO_x: Implications for Secondary Organic Aerosol Formation from Biomass Burning, *Environ. Sci. Technol.*, 52, 1981-1989, <https://doi.org/10.1021/acs.est.7b05864>, 2018.

Flannigan, M., Cantin, A. S., de Groot, W. J., Wotton, M., Newbery, A., and Gowman, L. M.: Global wildland fire season severity in the 21st century, *For. Ecol. Manag.*, 294, 54-61, <https://doi.org/10.1016/j.foreco.2012.10.022>, 2013.

Fried, A., Walega, J., Weibring, P., Richter, D., Simpson, I. J., Blake, D. R., Blake, N. J., Meinardi, S., Barletta, B., Hughes, S. C., Crawford, J. H., Diskin, G., Barrick, J., Hair, J., Fenn, M., Wisthaler, A., Mikoviny, T., Woo, J.-H., Park, M., Kim, J., Min, K.-E., Jeong, S., Wennberg, P. O., Kim, M. J., Crouse, J. D., Teng, A. P., Bennett, R., Yang-Martin, M., Shook, M. A., Huey, G., Tanner, D., Knote, C., Kim, J., Park, R., and Brune, W.: Airborne formaldehyde and volatile organic compound measurements over the Daesan petrochemical complex on Korea's northwest coast during the Korea-United States Air Quality study: Estimation of emission fluxes and effects on air quality, *Elem. Sci. Anth.*, 8:1, <https://doi.org/10.1525/elementa.2020.121>, 2020.

Gilman, J. B., Lerner, B. M., Kuster, W. C., Goldan, P. D., Warneke, C., Veres, P. R., Roberts, J. M., de Gouw, J. A., Burling, I. R., and Yokelson, R. J.: Biomass burning emissions and potential air quality impacts of volatile organic compounds and other trace gases from fuels common in the US, *Atmos. Chem. Phys.*, 15, 13915-13938, <https://doi.org/10.5194/acp-15-13915-2015>, 2015.

Griffin, D., McLinden, C. A., Dammers, E., Adams, C., Stockwell, C. E., Warneke, C., Bourgeois, I., Peischl, J., Ryerson, T. B., Zarzana, K. J., Rowe, J. P., Volkamer, R., Knote, C., Kille, N., Koenig, T. K., Lee, C. F., Rollins, D., Rickly, P. S., Chen, J., Fehr, L., Bourassa, A., Degenstein, D., Hayden, K., Mihele, C., Wren, S. N., Liggio, J., Akingunola, A., and Makar, P.: Biomass burning nitrogen dioxide emissions derived from space with TROPOMI: methodology and validation, *Atmos. Meas. Tech.*, 14, 7929-7957, <https://doi.org/10.5194/amt-14-7929-2021>, 2021.

Guo, H., Campuzano-Jost, P., Nault, B. A., Day, D. A., Schroder, J. C., Kim, D., Dibb, J. E., Dollner, M., Weinzierl, B., and Jimenez, J. L.: The importance of size ranges in aerosol instrument intercomparisons: a case study for the Atmospheric Tomography Mission, *Atmos. Meas. Tech.*, 14, 3631-3655, <https://doi.org/10.5194/amt-14-3631-2021>, 2021.

Hamilton, D. S., Hantson, S., Scott, C. E., Kaplan, J. O., Pringle, K. J., Nieradzik, L. P., Rap, A., Folberth, G. A., Spracklen, D. V., and Carslaw, K. S.: Reassessment of pre-industrial fire emissions strongly affects anthropogenic aerosol forcing, *Nat. Commun.*, 9, 3182, <https://doi.org/10.1038/s41467-018-05592-9>, 2018.

Deleted: et al.

923
924
925
926
927
928
929
930
931
932
933
934
935
936
937
938
939
940
941
942
943
944
945
946
947
948
949
950
951
952
953
954
955
956
957
958
959
960
961
962
963
964
965
966
967
968
969
970
971
972
973
974
975
976
977
978
979
980
981
982
983

Hatch, L. E., Yokelson, R. J., Stockwell, C. E., Veres, P. R., Simpson, I. J., Blake, D. R., Orlando, J. J., and Barsanti, K. C.: Multi-instrument comparison and compilation of non-methane organic gas emissions from biomass burning and implications for smoke-derived secondary organic aerosol precursors, *Atmos. Chem. Phys.*, 17, 1471-1489, <https://doi.org/10.5194/acp-17-1471-2017>, 2017.

Hodshire, A. L., Bian, Q., Ramnarine, E., Lonsdale, C. R., Alvarado, M. J., Kreidenweis, S. M., Jathar, S. H., and Pierce, J. R.: More Than Emissions and Chemistry: Fire Size, Dilution, and Background Aerosol Also Greatly Influence Near-Field Biomass Burning Aerosol Aging, *J. Geophys. Res. Atmos.*, 124, 5589-5611, <https://doi.org/10.1029/2018JD029674>, 2019.

Holder, A. L., Gullett, B. K., Urbanski, S. P., Elleman, R., O'Neill, S., Tabor, D., Mitchell, W., and Baker, K. R.: Emissions from prescribed burning of agricultural fields in the Pacific Northwest, *Atmos. Environ.*, 166, 22-33, <https://doi.org/10.1016/j.atmosenv.2017.06.043>, 2017.

Holmes, C. D., Fite, C., Agastra, A., Schwarz, J. P., Yokelson, R. J., Bui, T. V., and Peterson, D. A.: Critical evaluation of smoke age inferred from different methods during FIREX-AQ, <https://ui.adsabs.harvard.edu/abs/2020AGUFMA225.0010H>, 2020.

Isaacman-VanWertz, G., Sueper, D. T., Aikin, K. C., Lerner, B. M., Gilman, J. B., de Gouw, J. A., Worsnop, D. R., and Goldstein, A. H.: Automated single-ion peak fitting as an efficient approach for analyzing complex chromatographic data, *J. Chromatogr. A*, 1529, 81-92, <https://doi.org/10.1016/j.chroma.2017.11.005>, 2017.

Johnston, F. H., Henderson, S. B., Chen, Y., Randerson, J. T., Marlier, M., DeFries, R. S., Kinney, P., Bowman, D. M. J. S., and Brauer, M.: Estimated Global Mortality Attributable to Smoke from Landscape Fires, *Environ. Health Persp.*, 120, 695-701, <https://doi.org/10.1289/ehp.1104422>, 2012.

Jung, Y., González Abad, G., Nowlan, C. R., Chance, K., Liu, X., Torres, O., and Ahn, C.: Explicit Aerosol Correction of OMI Formaldehyde Retrievals, *Earth Space Sci.*, 6, 2087-2105, <https://doi.org/10.1029/2019EA000702>, 2019.

Keyword, M., Kanakidou, M., Stohl, A., Dentener, F., Grassi, G., Meyer, C. P., Torseth, K., Edwards, D., Thompson, A. M., Lohmann, U., and Burrows, J.: Fire in the Air: Biomass Burning Impacts in a Changing Climate, *Crit. Rev. i Environ. Sci. Technol.*, 43, 40-83, <https://doi.org/10.1080/10643389.2011.604248>, 2013.

Kloster, S., Mahowald, N. M., Randerson, J. T., Thornton, P. E., Hoffman, F. M., Levis, S., Lawrence, P. J., Feddema, J. J., Oleson, K. W., and Lawrence, D. M.: Fire dynamics during the 20th century simulated by the Community Land Model, *Biogeosciences*, 7, 1877-1902, <https://doi.org/10.5194/bg-7-1877-2010>, 2010.

Knorr, W., Dentener, F., Lamarque, J.-F., Jiang, L., and Arneeth, A.: Wildfire air pollution hazard during the 21st century, *Atmos. Chem. Phys.*, 17, 9223-9236, <https://doi.org/10.5194/acp-17-9223-2017>, 2017.

Kodros, J. K., Papanastasiou, D. K., Paglione, M., Masiol, M., Squizzato, S., Florou, K., Skyllakou, K., Kaltsonoudis, C., Nenes, A., and Pandis, S. N.: Rapid dark aging of biomass burning as an overlooked source of oxidized organic aerosol, *P. Natl. Acad. Sci. USA*, 117, 33028, <https://doi.org/10.1073/pnas.2010365117>, 2020.

Konovalov, I. B., Lvova, D. A., Beekmann, M., Jethva, H., Mikhailov, E. F., Paris, J. D., Belan, B. D., Kozlov, V. S., Ciaia, P., and Andreae, M. O.: Estimation of black carbon emissions from Siberian fires using satellite observations of absorption and extinction optical depths, *Atmos. Chem. Phys.*, 18, 14889-14924, <https://doi.org/10.5194/acp-18-14889-2018>, 2018.

Koss, A. R., Sekimoto, K., Gilman, J. B., Selimovic, V., Coggon, M. M., Zarzana, K. J., Yuan, B., Lerner, B. M., Brown, S. S., Jimenez, J. L., Krechmer, J., Roberts, J. M., Warneke, C., Yokelson, R. J., and de Gouw, J.: Non-methane organic gas emissions from biomass burning: identification, quantification, and emission factors from PTR-ToF during the FIREX 2016 laboratory experiment, *Atmos. Chem. Phys.*, 18, 3299-3319, <https://doi.org/10.5194/acp-18-3299-2018>, 2018.

Le Quéré, C., Andrew, R. M., Friedlingstein, P., Sitch, S., Hauck, J., Pongratz, J., Pickers, P. A., Korsbakken, J. I., Peters, G. P., Canadell, J. G., Arneeth, A., Arora, V. K., Barbero, L., Bastos, A., Bopp, L., Chevallier, F., Chini, L. P., Ciaia, P., Doney, S. C., Gkritzalis, T., Goll, D. S., Harris, I., Haverd, V., Hoffman, F. M., Hoppema, M., Houghton, R. A., Hurtt, G., Ilyina, T., Jain, A. K., Johannessen, T., Jones, C. D., Kato, E., Keeling, R. F., Goldewijk, K. K., Landschützer, P., Lefèvre, N., Lienert, S., Liu, Z., Lombardo, D., Metzl, N., Munro, D. R., Nabel, J. E. M. S.,

Deleted: and

Deleted: Science

Deleted: .

987 Nakaoka, S., Neill, C., Olsen, A., Ono, T., Patra, P., Peregón, A., Peters, W., Peylin, P., Pfeil, B., Pierrot, D., Poulter, B.,
988 Rehder, G., Resplandy, L., Robertson, E., Rocher, M., Rödenbeck, C., Schuster, U., Schwinger, J., Séférian, R.,
989 Skjelvan, I., Steinhoff, T., Sutton, A., Tans, P. P., Tian, H., Tilbrook, B., Tubiello, F. N., van der Laan-Luijkx, I. T., van
990 der Werf, G. R., Viovy, N., Walker, A. P., Wiltshire, A. J., Wright, R., Zechle, S., and Zheng, B.: Global Carbon Budget
991 2018, *Earth Syst. Sci. Data*, 10, 2141-2194, <https://doi.org/10.5194/essd-10-2141-2018>, 2018.

992
993 Lerner, B. M., Gilman, J. B., Aikin, K. C., Atlas, E. L., Goldan, P. D., Graus, M., Hendershot, R., Isaacman-VanWertz,
994 G. A., Koss, A., Kuster, W. C., Lueb, R. A., McLaughlin, R. J., Peischl, J., Sueper, D., Ryerson, T. B., Tokarek, T. W.,
995 Warneke, C., Yuan, B., and de Gouw, J. A.: An improved, automated whole air sampler and gas chromatography mass
996 spectrometry analysis system for volatile organic compounds in the atmosphere, *Atmos. Meas. Tech.*, 10, 291-313,
997 <https://doi.org/10.5194/amt-10-291-2017>, 2017.

998
999 Liao, J., Wolfe, G. M., Hannun, R. A., St. Clair, J. M., Hanisco, T. F., Gilman, J. B., Lamplugh, A., Selimovic, V.,
1000 Diskin, G. S., Nowak, J. B., Halliday, H. S., DiGangi, J. P., Hall, S. R., Ullmann, K., Holmes, C. D., Fite, C. H., Agastra,
1001 A., Ryerson, T. B., Peischl, J., Bourgeois, I., Warneke, C., Coggon, M. M., Gkatzelis, G. I., Sekimoto, K., Fried, A.,
1002 Richter, D., Weibring, P., Apel, E. C., Hornbrook, R. S., Brown, S. S., Womack, C. C., Robinson, M. A., Washenfelder,
1003 R. A., Veres, P. R., and Neuman, J. A.: Formaldehyde evolution in U.S. wildfire plumes during the Fire Influence on
1004 Regional to Global Environments and Air Quality experiment (FIREX-AQ), *Atmos. Chem. Phys.*, 21, 18319-18331,
1005 <https://doi.org/10.5194/acp-21-18319-2021>, 2021.

1006
1007 Lindaas, J., Pollack, I. B., Garofalo, L. A., Pothier, M. A., Farmer, D. K., Kreidenweis, S. M., Campos, T. L., Flocke, F.,
1008 Weinheimer, A. J., Montzka, D. D., Tyndall, G. S., Palm, B. B., Peng, Q., Thornton, J. A., Permar, W., Wielgasz, C., Hu,
1009 R., Ottmar, R. D., Restaino, J. C., Hudak, A. T., Ku, I. T., Zhou, Y., Sive, B. C., Sullivan, A., Collett Jr, J. L., and
1010 Fischer, E. V.: Emissions of Reactive Nitrogen From Western U.S. Wildfires During Summer 2018, *J. Geophys. Res.*
1011 *Atmos.*, 126, e2020JD032657, <https://doi.org/10.1029/2020JD032657>, 2021.

1012
1013 Ling, Z., Xie, Q., Shao, M., Wang, Z., Wang, T., Guo, H., and Wang, X.: Formation and sink of glyoxal and
1014 methylglyoxal in a polluted subtropical environment: observation-based photochemical analysis and impact evaluation,
1015 *Atmos. Chem. Phys.*, 20, 11451-11467, <https://doi.org/10.5194/acp-20-11451-2020>, 2020.

1016
1017 Liu, X., Huey, L. G., Yokelson, R. J., Selimovic, V., Simpson, I. J., Müller, M., Jimenez, J. L., Campuzano-Jost, P.,
1018 Beyersdorf, A. J., Blake, D. R., Butterfield, Z., Choi, Y., Crouse, J. D., Day, D. A., Diskin, G. S., Dubey, M. K.,
1019 Fortner, E., Hanisco, T. F., Hu, W., King, L. E., Kleinman, L., Meinardi, S., Mikoviny, T., Onasch, T. B., Palm, B. B.,
1020 Peischl, J., Pollack, I. B., Ryerson, T. B., Sachse, G. W., Sedlacek, A. J., Shilling, J. E., Springston, S., St. Clair, J. M.,
1021 Tanner, D. J., Teng, A. P., Wennberg, P. O., Wisthaler, A., and Wolfe, G. M.: Airborne measurements of western U.S.
1022 wildfire emissions: Comparison with prescribed burning and air quality implications, *J. Geophys. Res. Atmos.*, 122,
1023 6108-6129, <https://doi.org/10.1002/2016JD026315>, 2017.

1024
1025 Mann, M. L., Battlori, E., Moritz, M. A., Waller, E. K., Berck, P., Flint, A. L., Flint, L. E., and Dolfi, E.: Incorporating
1026 Anthropogenic Influences into Fire Probability Models: Effects of Human Activity and Climate Change on Fire Activity
1027 in California, *PLOS ONE*, 11, e0153589, <https://doi.org/10.1371/journal.pone.0153589>, 2016.

1028
1029 Martínez-Alonso, S., Deeter, M., Worden, H., Borsdorff, T., Aben, I., Commane, R., Daube, B., Francis, G., George, M.,
1030 Landgraf, J., Mao, D., McKain, K., and Wofsy, S.: 1.5 years of TROPOMI CO measurements: comparisons to MOPITT
1031 and ATom, *Atmos. Meas. Tech.*, 13, 4841-4864, <https://doi.org/10.5194/amt-13-4841-2020>, 2020.

1032
1033 Min, K. E., Washenfelder, R. A., Dubé, W. P., Langford, A. O., Edwards, P. M., Zarzana, K. J., Stutz, J., Lu, K., Rohrer,
1034 F., Zhang, Y., and Brown, S. S.: A broadband cavity enhanced absorption spectrometer for aircraft measurements of
1035 glyoxal, methylglyoxal, nitrous acid, nitrogen dioxide, and water vapor, *Atmos. Meas. Tech.*, 9, 423-440,
1036 <https://doi.org/10.5194/amt-9-423-2016>, 2016.

1037
1038 Mitsuishi, K., Iwasaki, M., Takeuchi, M., Okochi, H., Kato, S., Ohira, S.-I., and Toda, K.: Diurnal Variations in
1039 Partitioning of Atmospheric Glyoxal and Methylglyoxal between Gas and Particles at the Ground Level and in the Free
1040 Troposphere, *ACS Earth Space Chem.*, 2, 915-924, <https://doi.org/10.1021/acsearthspacechem.8b00037>, 2018.

1041
1042 Moritz, M. A., Parisien, M.-A., Battlori, E., Krawchuk, M. A., Van Dorn, J., Ganz, D. J., and Hayhoe, K.: Climate
1043 change and disruptions to global fire activity, *Ecosphere*, 3, 49, <https://doi.org/10.1890/ES11-00345.1>, 2012.

1044
1045 Mouat, A. P., Paton-Walsh, C., Simmons, J. B., Ramirez-Gamboa, J., Griffith, D. W. T., and Kaiser, J.: [Measurement](#)
1046 [report: Observations of long-lived volatile organic compounds from the 2019-2020 Australian wildfires during the](#)
1047 [COALA campaign](#), *Atmos. Chem. Phys.*, 2022, 22, 11033-11047, <https://doi.org/10.5194/acp-22-11033-2022>, 2022.

Deleted: Emission factors

Deleted: Discuss.

Deleted: 2021, 1-13, <https://doi.org/10.5194/acp-2021-742>, 2021...

1052
1053 Müller, M., Anderson, B. E., Beyersdorf, A. J., Crawford, J. H., Diskin, G. S., Eichler, P., Fried, A., Keutsch, F. N.,
1054 Mikoviny, T., Thornhill, K. L., Walega, J. G., Weinheimer, A. J., Yang, M., Yokelson, R. J., and Wisthaler, A.: In situ
1055 measurements and modeling of reactive trace gases in a small biomass burning plume, *Atmos. Chem. Phys.*, 16, 3813-
1056 3824, <https://doi.org/10.5194/acp-16-3813-2016>, 2016.

1057
1058 NASA airborne science data for atmospheric composition, <https://doi.org/10.5067/suborbital/firexaq2019/data001>, 2019.

1059
1060 National Interagency Fire Center; Internetseite vom 24.10.2015: Total Wildland Fires and Acres (1960-2009).
1061 http://www.nifc.gov/fireInfo/fireInfo_stats_totalFires.html, <https://www.nifc.gov/fire-information/statistics/wildfires>,
1062 <https://www.nifc.gov/fire-information/statistics/prescribed-fire>

1063
1064 Olivier, J. G. J., Van Aardenne, J. A., Dentener, F. J., Pagliari, V., Ganzeveld, L. N., and Peters, J. A. H. W.: Recent
1065 trends in global greenhouse gas emissions: regional trends 1970–2000 and spatial distribution of key sources in 2000,
1066 *Environmental Sciences*, 2, 81-99, <https://doi.org/10.1080/15693430500400345>, 2005.

1067
1068 Pagonis, D., Sekimoto, K. and de Gouw, J. A.: A library of proton-transfer reactions of H₃O⁺ ions used for trace gas
1069 detection, *J. Am. Soc. Mass Spectrom.*, 30, 1330–1335, <https://doi.org/10.1007/s13361-019-02209-3>, 2019.

1070
1071 Pagonis, D., Campuzano-Jost, P., Guo, H., Day, D. A., Schueneman, M., Nault, B. A., Brown, W., Laskin, A., Siemens,
1072 K. S. A., Coggon, M. M., DiGangi, J. P., Diskin, G. S., Fenn, M. A., Gkatzelis, G., Hair, J. W., Halliday, H. S., Katich, J.
1073 M., Nowak, J. B., Perring, A. E., Saide, P. E., Sekimoto, K., Shingler, T. J., Thapa, L., Warneke, C., and Jimenez, J. L.:
1074 Chemical Aging of Biomass Burning Organic Aerosol: Insight from Fast Near-Molecular Measurements, December 01,
1075 2020.

1076
1077 Pagonis, D., Campuzano-Jost, P., Guo, H., Day, D. A., Schueneman, M. K., Brown, W. L., Nault, B. A., Stark, H.,
1078 Siemens, K., Laskin, A., Piel, F., Tomsche, L., Wisthaler, A., Coggon, M. M., Gkatzelis, G. I., Halliday, H. S.,
1079 Krechmer, J. E., Moore, R. H., Thomson, D. S., Warneke, C., Wiggins, E. B., and Jimenez, J. L.: Airborne extractive
1080 electrospray mass spectrometry measurements of the chemical composition of organic aerosol, *Atmos. Meas. Tech.*, 14,
1081 1545-1559, <https://doi.org/10.5194/amt-14-1545-2021>, 2021.

1082
1083 Pechony, O. and Shindell, D. T.: Driving forces of global wildfires over the past millennium and the forthcoming
1084 century, *P. Natl. Acad. Sci. USA*, 107, 19167, <https://doi.org/10.1073/pnas.1003669107>, 2010.

1085
1086 Peng, Q., Palm, B. B., Melander, K. E., Lee, B. H., Hall, S. R., Ullmann, K., Campos, T., Weinheimer, A. J., Apel, E. C.,
1087 Hornbrook, R. S., Hills, A. J., Montzka, D. D., Flocke, F., Hu, L., Permar, W., Wielgasz, C., Lindaas, J., Pollack, I. B.,
1088 Fischer, E. V., Bertram, T. H., and Thornton, J. A.: HONO Emissions from Western U.S. Wildfires Provide Dominant
1089 Radical Source in Fresh Wildfire Smoke, *Environ. Sci. Technol.*, 54, 5954-5963,
1090 <https://doi.org/10.1021/acs.est.0c00126>, 2020.

1091
1092 Permar, W., Wang, Q., Selimovic, V., Wielgasz, C., Yokelson, R. J., Hornbrook, R. S., Hills, A. J., Apel, E. C., Ku, I. T.,
1093 Zhou, Y., Sive, B. C., Sullivan, A. P., Collett Jr, J. L., Campos, T. L., Palm, B. B., Peng, Q., Thornton, J. A., Garofalo,
1094 L. A., Farmer, D. K., Kreidenweis, S. M., Levin, E. J. T., DeMott, P. J., Flocke, F., Fischer, E. V., and Hu, L.: Emissions
1095 of Trace Organic Gases From Western U.S. Wildfires Based on WE-CAN Aircraft Measurements, *J. Geophys. Res.*
1096 *Atmos.*, 126, e2020JD033838, <https://doi.org/10.1029/2020JD033838>, 2021.

1097
1098 Prichard, S. J., O'Neill, S. M., Eagle, P., Andreu, A. G., Drye, B., Dubowy, J., Urbanski, S., and Strand, T. M.: Wildland
1099 fire emission factors in North America: synthesis of existing data, measurement needs and management applications, *Int.*
1100 *J. Wildland Fire*, 29, 132-147, <https://doi.org/10.1071/WF19066>, 2020.

1101
1102 Reddington, C. L., Spracklen, D. V., Artaxo, P., Ridley, D. A., Rizzo, L. V., and Arana, A.: Analysis of particulate
1103 emissions from tropical biomass burning using a global aerosol model and long-term surface observations, *Atmos.*
1104 *Chem. Phys.*, 16, 11083-11106, <https://doi.org/10.5194/acp-16-11083-2016>, 2016.

1105
1106 Richter, D., Weibring, P., Walega, J. G., Fried, A., Spuler, S. M., and Taubman, M. S.: Compact highly sensitive multi-
1107 species airborne mid-IR spectrometer, *Appl. Phys. B.*, <https://doi.org/10.1007/s00340-015-6038-8>, 2015.

1108
1109 Rickly, P., Guo, H., Campuzano-Jost, P., Jimenez, J. L., Wolfe, G. M., Bennett, R., Bourgeois, I., Crouse, J. D., Dibb, J.
1110 E., DiGangi, J. P., Diskin, G. S., Dollner, M., Gargulinski, E. M., Hall, S. R., Halliday, H. S., Hanisco, T. F., Hannun, R.
1111 A., Liao, J., Moore, R., Nault, B. A., Nowak, J. B., Robinson, C. E., Ryerson, T., Sanchez, K. J., Schöberl, M., Soja, A.
1112 J., St. Clair, J. M., Thornhill, K. L., Ullmann, K., Wennberg, P. O., Weinzierl, B., Wiggins, E. B., Winstead, E. L., and

1113 Rollins, A. W.: Emission factors and evolution of SO₂ measured from biomass burning in wild and agricultural fires,
 1114 Atmos. Chem. Phys., 2022, 22, 15603-15620, <https://doi.org/10.5194/acp-22-15603-2022>, 2022.

1115

1116 Roberts, J. M., Stockwell, C. E., Yokelson, R. J., de Gouw, J., Liu, Y., Selimovic, V., Koss, A. R., Sekimoto, K.,
 1117 Coggon, M. M., Yuan, B., Zarzana, K. J., Brown, S. S., Santin, C., Doerr, S. H., and Warneke, C.: The nitrogen budget
 1118 of laboratory-simulated western US wildfires during the FIREX 2016 Fire Lab study, Atmos. Chem. Phys., 20, 8807-
 1119 8826, <https://doi.org/10.5194/acp-20-8807-2020>, 2020.

1120

1121 Robinson, M. A., Neuman, J. A., Huey, L. G., Roberts, J. M., Brown, S. S., and Veres, P. R.: Temperature-dependent
 1122 sensitivity of iodide chemical ionization mass spectrometers, Atmos. Meas. Tech., 15, 4295-4305,
 1123 <https://doi.org/10.5194/amt-15-4295-2022>, 2022.

1124

1125 Robinson, M. A., Decker, Z. C. J., Barsanti, K. C., Coggon, M. M., Flocke, F. M., Franchin, A., Fredrickson, C. D.,
 1126 Gilman, J. B., Gkatzelis, G. I., Holmes, C. D., Lamplugh, A., Lavi, A., Middlebrook, A. M., Montzka, D. M., Palm, B.
 1127 B., Peischl, J., Pierce, B., Schwantes, R. H., Sekimoto, K., Selimovic, V., Tyndall, G. S., Thornton, J. A., Van Rooy, P.,
 1128 Warneke, C., Weinheimer, A. J., and Brown, S. S.: Variability and Time of Day Dependence of Ozone Photochemistry
 1129 in Western Wildfire Plumes, Environ. Sci. Technol., 55, 10280-10290, <https://doi.org/10.1021/acs.est.1c01963>, 2021.

1130

1131 Rollins, A. W., Rickly, P. S., Gao, R. S., Ryerson, T. B., Brown, S. S., Peischl, J., and Bourgeois, I.: Single-photon laser-
 1132 induced fluorescence detection of nitric oxide at sub-parts-per-trillion mixing ratios, Atmos. Meas. Tech., 13, 2425-2439,
 1133 <https://doi.org/10.5194/amt-13-2425-2020>, 2020.

1134

1135 Ryerson, T. B., Williams, E. J., and Fehsenfeld, F. C.: An efficient photolysis system for fast-response NO₂
 1136 measurements, *J. of Geophys. Res.: Atmos.*, 105, 26447-26461, <https://doi.org/10.1029/2000JD900389>, 2000.

1137

1138 Sachse, G. W., Collins, J., Hill, G. F., Wade, L. O., Burney, L. G., and Ritter, J. A.: Airborne tunable diode laser sensor
 1139 for high-precision concentration and flux measurements of carbon monoxide and methane, Photonics West - Lasers and
 1140 Applications in Science and Engineering, <https://doi.org/10.1117/12.46162>, 1991.

1141

1142 Sachse, S. W., Collins, J. E., Hill, G. F., Wade, L. O., Burney, L. G., and Ritter, J. A.: Airborne tunable diode laser
 1143 sensor for high-precision concentration and flux measurements of carbon monoxide and methane, Proc.SPIE, 1991.

1144 Schwarz, J. P., Gao, R. S., Spackman, J. R., Watts, L. A., Thomson, D. S., Fahey, D. W., Ryerson, T. B., Peischl, J.,
 1145 Holloway, J. S., Trainer, M., Frost, G. J., Baynard, T., Lack, D. A., de Gouw, J. A., Warneke, C., and Del Negro, L. A.:
 1146 Measurement of the mixing state, mass, and optical size of individual black carbon particles in urban and biomass
 1147 burning emissions, Geophys. Res. Lett., 35, L13810, <https://doi.org/10.1029/2008gl033968>, 2008.

1148

1149 Schneising, O., Buchwitz, M., Reuter, M., Bovensmann, H., and Burrows, J. P.: Severe Californian wildfires in
 1150 November 2018 observed from space: the carbon monoxide perspective, Atmos. Chem. Phys., 20, 3317-3332,
 1151 <https://doi.org/10.5194/acp-20-3317-2020>, 2020.

1152

1153 Schwarz, J. P., Spackman, J. R., Fahey, D. W., Gao, R. S., Lohmann, U., Stier, P., Watts, L. A., Thomson, D. S., Lack,
 1154 D. A., Pfister, L., Mahoney, M. J., Baumgardner, D., Wilson, J. C., and Reeves, J. M.: Coatings and their enhancement
 1155 of black carbon light absorption in the tropical atmosphere, J. Geophys. Res. Atmos., 113, D03203,
 1156 <https://doi.org/10.1029/2007JD009042>, 2008.

1157

1158 Sekimoto, K., Li, S.-M., Yuan, B., Koss, A., Coggon, M., Warneke, C., and de Gouw, J.: Calculation of the sensitivity of
 1159 proton-transfer-reaction mass spectrometry (PTR-MS) for organic trace gases using molecular properties, Int. J. Mass
 1160 Spectrom., 421, 71-94, <https://doi.org/10.1016/j.ijms.2017.04.006>, 2017.

1161

1162 Sekimoto, K., Koss, A. R., Gilman, J. B., Selimovic, V., Coggon, M. M., Zarzana, K. J., Yuan, B., Lerner, B. M., Brown,
 1163 S. S., Warneke, C., Yokelson, R. J., Roberts, J. M., and de Gouw, J.: High- and low-temperature pyrolysis profiles
 1164 describe volatile organic compound emissions from western US wildfire fuels, Atmos. Chem. Phys., 18, 9263-9281,
 1165 <https://doi.org/10.5194/acp-18-9263-2018>, 2018.

1166

1167 Selimovic, V., Yokelson, R. J., Warneke, C., Roberts, J. M., de Gouw, J., Reardon, J., and Griffith, D. W. T.: Aerosol
 1168 optical properties and trace gas emissions by PAX and OP-FTIR for laboratory-simulated western US wildfires during
 1169 FIREX, Atmos. Chem. Phys., 18, 2929-2948, <https://doi.org/10.5194/acp-18-2929-2018>, 2018.

1170

1171 Shrivastava, M., Cappa, C. D., Fan, J., Goldstein, A. H., Guenther, A. B., Jimenez, J. L., Kuang, C., Laskin, A., Martin,
 1172 S. T., Ng, N. L., Petaja, T., Pierce, J. R., Rasch, P. J., Roldin, P., Seinfeld, J. H., Shilling, J., Smith, J. N., Thornton, J. A.,
 1173 Volkamer, R., Wang, J., Worsnop, D. R., Zaveri, R. A., Zelenyuk, A., and Zhang, Q.: Recent advances in understanding

Deleted: Discuss., 2022, 1-29, <https://doi.org/10.5194/acp-2022-309>, 2022.

Deleted: Journal

Deleted: Geophysical

Deleted: Research

Deleted: Atmospheres

1180 secondary organic aerosol: Implications for global climate forcing, *Rev. Geophys.*, 55, 509-559,
 1181 <https://doi.org/10.1002/2016RG000540>, 2017.

1182

1183 Simpson, I. J., Colman, J. J., Swanson, A. L., Bandy, A. R., Thornton, D. C., Blake, D. R., and Rowland, F. S.: Aircraft
 1184 Measurements of Dimethyl Sulfide (DMS) Using a Whole Air Sampling Technique, *J. Atmos. Chem.*, 39, 191-213,
 1185 <https://doi.org/10.1023/A:1010608529779>, 2001.

1186

1187 Simpson, I. J., Blake, D. R., Blake, N. J., Meinardi, S., Barletta, B., Hughes, S. C., Fleming, L. T., Crawford, J. H.,
 1188 Diskin, G. S., Emmons, L. K., Fried, A., Guo, H., Peterson, D. A., Wisthaler, A., Woo, J.-H., Barré, J., Gaubert, B., Kim,
 1189 J., Kim, M. J., Kim, Y., Knote, C., Mikoviny, T., Pusede, S. E., Schroeder, J. R., Wang, Y., Wennberg, P. O., and Zeng,
 1190 L.: Characterization, sources and reactivity of volatile organic compounds (VOCs) in Seoul and surrounding regions
 1191 during KORUS-AQ, *Elementa: Science of the Anthropocene*, 8, <https://doi.org/10.1525/elementa.434>, 2020.

1192

1193 Spracklen, D. V., Mickley, L. J., Logan, J. A., Hudman, R. C., Yevich, R., Flannigan, M. D., and Westerling, A. L.:
 1194 Impacts of climate change from 2000 to 2050 on wildfire activity and carbonaceous aerosol concentrations in the
 1195 western United States, *J. Geophys. Res. Atmos.*, 114, <https://doi.org/10.1029/2008JD010966>, 2009.

1196

1197 Stark, H., Yatavelli, R. L. N., Thompson, S. L., Kimmel, J. R., Cubison, M. J., Chhabra, P. S., Canagaratna, M. R.,
 1198 Jayne, J. T., Worsnop, D. R., and Jimenez, J. L.: Methods to extract molecular and bulk chemical information from series
 1199 of complex mass spectra with limited mass resolution, *Int. J. Mass Spectrom.*, 389, 26-38,
 1200 <https://doi.org/10.1016/j.ijms.2015.08.011>, 2015.

1201

1202 Stockwell, C. E., Yokelson, R. J., Kreidenweis, S. M., Robinson, A. L., DeMott, P. J., Sullivan, R. C., Reardon, J., Ryan,
 1203 K. C., Griffith, D. W. T., and Stevens, L.: Trace gas emissions from combustion of peat, crop residue, domestic biofuels,
 1204 grasses, and other fuels: configuration and Fourier transform infrared (FTIR) component of the fourth Fire Lab at
 1205 Missoula Experiment (FLAME-4), *Atmos. Chem. Phys.*, 14, 9727-9754, <https://doi.org/10.5194/acp-14-9727-2014>,
 1206 2014.

1207

1208 Stockwell, C. E., Veres, P. R., Williams, J., and Yokelson, R. J.: Characterization of biomass burning emissions from
 1209 cooking fires, peat, crop residue, and other fuels with high-resolution proton-transfer-reaction time-of-flight mass
 1210 spectrometry, *Atmos. Chem. Phys.*, 15, 845-865, <https://doi.org/10.5194/acp-15-845-2015>, 2015.

1211

1212 Stockwell, C. E., Jayarathne, T., Cochrane, M. A., Ryan, K. C., Putra, E. I., Saharjo, B. H., Nurhayati, A. D., Albar, I.,
 1213 Blake, D. R., Simpson, I. J., Stone, E. A., and Yokelson, R. J.: Field measurements of trace gases and aerosols emitted by
 1214 peat fires in Central Kalimantan, Indonesia, during the 2015 El Niño, *Atmos. Chem. Phys.*, 16, 11711-11732,
 1215 <https://doi.org/10.5194/acp-16-11711-2016>, 2016.

1216

1217 Stöner, C., Derstroff, B., Klüpfel, T., Crowley, J. N., and Williams, J.: Glyoxal measurement with a proton transfer
 1218 reaction time of flight mass spectrometer (PTR-TOF-MS): characterization and calibration, *J. Mass Spectrom.*, 52, 30-
 1219 35, <https://doi.org/10.1002/jms.3893>, 2017.

1220

1221 Sudo, K. and Akimoto, H.: Global source attribution of tropospheric ozone: Long-range transport from various source
 1222 regions, *J. Geophys. Res. Atmos.*, 112, <https://doi.org/10.1029/2006JD007992>, 2007.

1223

1224 Theys, N., Volkamer, R., Müller, J. F., Zarzana, K. J., Kille, N., Clarisse, L., De Smedt, I., Lerot, C., Finkenzeller, H.,
 1225 Hendrick, F., Koenig, T. K., Lee, C. F., Knote, C., Yu, H., and Van Roozendaal, M.: Global nitrous acid emissions and
 1226 levels of regional oxidants enhanced by wildfires, *Nat. Geosci.*, 13, 681-686, <https://doi.org/10.1038/s41561-020-0637-7>,
 1227 2020.

1228

1229 Tomsche, L., Piel, F., Mikoviny, T., Nielsen, C. J., Guo, H., Campuzano-Jost, P., Nault, B. A., Schueneman, M. K.,
 1230 Jimenez, J. L., Halliday, H., Diskin, G., DiGangi, J. P., Nowak, J. B., Wiggins, E. B., Gargulinski, E., Soja, A. J., and
 1231 Wisthaler, A.: Measurement report: Emission factors of NH₃ and NH_x for wildfires and agricultural fires in the United
 1232 States, *Atmos. Chem. Phys.*, 23, 2331-2343, <https://doi.org/10.5194/acp-23-2331-2023>, 2023.

1233

1234 Thornhill, G. D., Ryder, C. L., Highwood, E. J., Shaffrey, L. C., and Johnson, B. T.: The effect of South American
 1235 biomass burning aerosol emissions on the regional climate, *Atmos. Chem. Phys.*, 18, 5321-5342,
 1236 <https://doi.org/10.5194/acp-18-5321-2018>, 2018.

1237

1238 Tian, H., Lu, C., Ciais, P., Michalak, A. M., Canadell, J. G., Saikawa, E., Huntzinger, D. N., Gurney, K. R., Sitch, S.,
 1239 Zhang, B., Yang, J., Bousquet, P., Bruhwiler, L., Chen, G., Dlugokencky, E., Friedlingstein, P., Melillo, J., Pan, S.,

Deleted: .

Deleted: .

- 1242 Poulter, B., Prinn, R., Saunois, M., Schwalm, C. R., and Wofsy, S. C.: The terrestrial biosphere as a net source of
1243 greenhouse gases to the atmosphere, *Nature*, 531, 225-228, <https://doi.org/10.1038/nature16946>, 2016.
- 1244
- 1245 Tsimpidi, A. P., Karydis, V. A., Pandis, S. N., and Lelieveld, J.: Global-scale combustion sources of organic aerosols:
1246 sensitivity to formation and removal mechanisms, *Atmos. Chem. Phys.*, 17, 7345-7364, <https://doi.org/10.5194/acp-17-7345-2017>, 2017.
- 1247
- 1248
- 1249 Urbanski, S. P., Hao, W. M. and Baker, S.: Chapter 4 Chemical Composition of Wildland Fire Emissions, *Dev. Environ.*
1250 *Sci.*, 8, 79-107, [https://doi.org/10.1016/S1474-8177\(08\)00004-1](https://doi.org/10.1016/S1474-8177(08)00004-1), 2008.
- 1251
- 1252 Vasilkov, A., Krotkov, N., Yang, E. S., Lamsal, L., Joiner, J., Castellanos, P., Fasnacht, Z., and Spurr, R.: Explicit and
1253 consistent aerosol correction for visible wavelength satellite cloud and nitrogen dioxide retrievals based on optical
1254 properties from a global aerosol analysis, *Atmos. Meas. Tech.*, 14, 2857-2871, <https://doi.org/10.5194/amt-14-2857-2021>, 2021.
- 1255
- 1256
- 1257 Vay, S. A., Tyler, S. C., Choi, Y., Blake, D. R., Blake, N. J., Sachse, G. W., Diskin, G. S., and Singh, H. B.: Sources and
1258 transport of $\Delta^{14}\text{C}$ in CO_2 within the Mexico City Basin and vicinity, *Atmos. Chem. Phys.*, 9, 4973-4985,
1259 <https://doi.org/10.5194/acp-9-4973-2009>, 2009.
- 1260
- 1261 Veres, P. R., Neuman, J. A., Bertram, T. H., Assaf, E., Wolfe, G. M., Williamson, C. J., Weinzierl, B., Tilmes, S.,
1262 Thompson, C. R., Thames, A. B., Schroder, J. C., Saiz-Lopez, A., Rollins, A. W., Roberts, J. M., Price, D., Peischl, J.,
1263 Nault, B. A., Møller, K. H., Miller, D. O., Meinardi, S., Li, Q., Lamarque, J.-F., Kupc, A., Kjaergaard, H. G., Kinnison,
1264 D., Jimenez, J. L., Jernigan, C. M., Hornbrook, R. S., Hills, A., Dollner, M., Day, D. A., Cuevas, C. A., Campuzano-Jost,
1265 P., Burkholder, J., Bui, T. P., Brune, W. H., Brown, S. S., Brock, C. A., Bourgeois, I., Blake, D. R., Apel, E. C., and
1266 Ryerson, T. B.: Global airborne sampling reveals a previously unobserved dimethyl sulfide oxidation mechanism in the
1267 marine atmosphere, *P. Natl. Acad. Sci.*, 117, 4505, <https://doi.org/10.1073/pnas.1919344117>, 2020.
- 1268
- 1269 Wang, S., Coggon, M. M., Gkatzelis, G. I., Warneke, C., Bourgeois, I., Ryerson, T. B., Peischl, J., Veres, P. R., Neuman,
1270 J. A., Hair, J., Shingler, T., Fenn, M., Diskin, G., Huey, L. G., Lee, Y. R., Apel, E. C., Hornbrook, R. S., Hills, A. J.,
1271 Hall, S. R., Ullmann, K., Bela, M. M., Trainer, M. K., Kumar, R., Orlando, J. J., Flocke, F. M., and Emmons, L. K.:
1272 Chemical Tomography in a Fresh Wildland Fire Plume: a Large Eddy Simulation (LES) Study, *J. Geophys. Res. Atmos.*,
1273 126, e2021JD035203, <https://doi.org/10.1029/2021JD035203>, 2021.
- 1274
- 1275 Ward, D. S., Kloster, S., Mahowald, N. M., Rogers, B. M., Randerson, J. T., and Hess, P. G.: The changing radiative
1276 forcing of fires: global model estimates for past, present and future, *Atmos. Chem. Phys.*, 12, 10857-10886,
1277 <https://doi.org/10.5194/acp-12-10857-2012>, 2012.
- 1278
- 1279 Warneke, C., Roberts, J. M., Veres, P., Gilman, J., Kuster, W. C., Burling, I., Yokelson, R., and de Gouw, J. A.: VOC
1280 identification and inter-comparison from laboratory biomass burning using PTR-MS and PIT-MS, *Int. J. Mass*
1281 *Spectrom.*, 303, 6-14, <https://doi.org/10.1016/j.ijms.2010.12.002>, 2011.
- 1282
- 1283 [Warneke, C., Schwarz, J. P., Dibb, J., Kalashnikova, O., Frost, G., Al-Saad, J., Brown, S. S., Brewer, W. A., Soja, A.,
1284 Seidel, F. C., Washenfelder, R. A., Wiggins, E. B., Moore, R. H., Anderson, B. E., Jordan, C., Yacovitch, T. I., Herndon,
1285 S. C., Liu, S., Kuwayama, T., Jaffe, D., Johnston, N., Selimovic, V., Yokelson, R., Giles, D. M., Holben, B. N., Goloub,
1286 P., Popovici, I., Trainer, M., Kumar, A., Pierce, R. B., Fahey, D., Roberts, J., Gargulinski, E. M., Peterson, D. A., Ye, X.,
1287 Thapa, L. H., Saide, P. E., Fite, C. H., Holmes, C. D., Wang, S., Coggon, M. M., Decker, Z. C. J., Stockwell, C. E., Xu,
1288 L., Gkatzelis, G., Aikin, K., Lefer, B., Kaspari, J., Griffin, D., Zeng, L., Weber, R., Hastings, M., Chai, J., Wolfe, G. M.,
1289 Hanco, T. F., Liao, J., Campuzano Jost, P., Guo, H., Jimenez, J. L., Crawford, J., and The, F.-A. Q. S. T.: Fire
1290 Influence on Regional to Global Environments and Air Quality \(FIREX-AQ\), *J. of Geophys. Res.: Atmos.*, 128,
1291 e2022JD037758, <https://doi.org/10.1029/2022JD037758>, 2023.](https://doi.org/10.1029/2022JD037758)
- 1292
- 1293 Weibring, P., Richter, D., Walega, J. G., and Fried, A.: First demonstration of a high performance difference frequency
1294 spectrometer on airborne platforms, *Opt. Express*, 15, 13476-13495, <https://doi.org/10.1364/OE.15.013476>, 2007.
- 1295
- 1296 Westerling, A. L., Hidalgo, H. G., Cayan, D. R., and Swetnam, T. W.: Warming and Earlier Spring Increase Western
1297 U.S. Forest Wildfire Activity, *Science*, 313, 940, <https://doi.org/10.1126/science.1128834>, 2006.
- 1298
- 1299 Wiedinmyer, C. and Hurteau, M. D.: Prescribed Fire As a Means of Reducing Forest Carbon Emissions in the Western
1300 United States, *Environ. Sci. Technol.*, 44, 1926-1932, <https://doi.org/10.1021/es902455e>, 2010.
- 1301

1302 Wiedinmyer, C., Akagi, S. K., Yokelson, R. J., Emmons, L. K., Al-Saadi, J. A., Orlando, J. J., and Soja, A. J.: The Fire
1303 INventory from NCAR (FINN): a high resolution global model to estimate the emissions from open burning, *Geosci.*
1304 *Model Dev.*, 4, 625-641, <https://doi.org/10.5194/gmd-4-625-2011>, 2011.

1305
1306 Wiggins, E. B., Soja, A. J., Gargulinski, E., Halliday, H. S., Pierce, R. B., Schmidt, C. C., Nowak, J. B., DiGangi, J. P.,
1307 Diskin, G. S., Katic, J. M., Perring, A. E., Schwarz, J. P., Anderson, B. E., Chen, G., Crosbie, E. C., Jordan, C.,
1308 Robinson, C. E., Sanchez, K. J., Shingler, T. J., Shook, M., Thornhill, K. L., Winstead, E. L., Ziemba, L. D., and Moore,
1309 R. H.: High Temporal Resolution Satellite Observations of Fire Radiative Power Reveal Link Between Fire Behavior
1310 and Aerosol and Gas Emissions, *Geophys. Res. Lett.*, 47, e2020GL090707, <https://doi.org/10.1029/2020GL090707>,
1311 2020.

1312
1313 Wolfe, G. M., Hanisco, T. F., Arkinson, H. L., Blake, D. R., Wisthaler, A., Mikoviny, T., Ryerson, T. B., Pollack, I.,
1314 Peischl, J., Wennberg, P. O., Crouse, J. D., St. Clair, J. M., Teng, A., Huey, L. G., Liu, X., Fried, A., Weibring, P.,
1315 Richter, D., Walega, J., Hall, S. R., Ullmann, K., Jimenez, J. L., Campuzano-Jost, P., Bui, T. P., Diskin, G., Podolske, J.
1316 R., Sachse, G., and Cohen, R. C.: Photochemical evolution of the 2013 California Rim Fire: synergistic impacts of
1317 reactive hydrocarbons and enhanced oxidants, *Atmos. Chem. Phys.*, 22, 4253-4275, [https://doi.org/10.5194/acp-22-](https://doi.org/10.5194/acp-22-4253-2022)
1318 [4253-2022](https://doi.org/10.5194/acp-22-4253-2022), 2022.

1319
1320 [Xu, L., Crouse, J. D., Vasquez, K. T., Allen, H., Wennberg, P. O., Bourgeois, I., Brown, S. S., Campuzano-Jost, P.,](https://doi.org/10.5194/acp-22-4253-2022)
1321 [Coggon, M. M., Crawford, J. H., DiGangi, J. P., Diskin, G. S., Fried, A., Gargulinski, E. M., Gilman, J. B., Gkatzelis, G.](https://doi.org/10.5194/acp-22-4253-2022)
1322 [L., Guo, H., Hair, J. W., Hall, S. R., Halliday, H. A., Hanisco, T. F., Hannun, R. A., Holmes, C. D., Huey, L. G., Jimenez,](https://doi.org/10.5194/acp-22-4253-2022)
1323 [J. L., Lamplugh, A., Lee, Y. R., Liao, J., Lindaas, J., Neuman, J. A., Nowak, J. B., Peischl, J., Peterson, D. A., Piel, F.,](https://doi.org/10.5194/acp-22-4253-2022)
1324 [Richter, D., Rickly, P. S., Robinson, M. A., Rollins, A. W., Ryerson, T. B., Sekimoto, K., Selimovic, V., Shingler, T.,](https://doi.org/10.5194/acp-22-4253-2022)
1325 [Soja, A. J., St. Clair, J. M., Tanner, D. J., Ullmann, K., Veres, P. R., Walega, J., Warneke, C., Washenfelder, R. A.,](https://doi.org/10.5194/acp-22-4253-2022)
1326 [Weibring, P., Wisthaler, A., Wolfe, G. M., Womack, C. C., and Yokelson, R. J.: Ozone chemistry in western U.S.](https://doi.org/10.5194/acp-22-4253-2022)
1327 [wildfire plumes, *Sci. Adv.*, 7, eab13648, <https://doi.org/10.1126/sciadv.abl3648>, 2021.](https://doi.org/10.5194/acp-22-4253-2022)

1328
1329 ▼ van der Velde, I. R., van der Werf, G. R., Houweling, S., Eskes, H. J., Veeckind, J. P., Borsdorff, T., and Aben, I.:
1330 Biomass burning combustion efficiency observed from space using measurements of CO and NO₂ by the
1331 TROPOspheric Monitoring Instrument (TROPOMI), *Atmos. Chem. Phys.*, 21, 597-616, [https://doi.org/10.5194/acp-21-](https://doi.org/10.5194/acp-21-597-2021)
1332 [597-2021](https://doi.org/10.5194/acp-21-597-2021), 2021.

1333
1334 Yokelson, R. J., Griffith, D. W. T., and Ward, D. E.: Open-path Fourier transform infrared studies of large-scale
1335 laboratory biomass fires, *J. Geophys. Res. Atmos.*, 101, 21067-21080, <https://doi.org/10.1029/96JD01800>, 1996.

1336
1337 Yokelson, R. J., Christian, T. J., Karl, T. G., and Guenther, A.: The tropical forest and fire emissions experiment:
1338 laboratory fire measurements and synthesis of campaign data, *Atmos. Chem. Phys.*, 8, 3509-3527,
1339 <https://doi.org/10.5194/acp-8-3509-2008>, 2008.

1340
1341 Yokelson, R. J., Burling, I. R., Gilman, J. B., Warneke, C., Stockwell, C. E., de Gouw, J., Akagi, S. K., Urbanski, S. P.,
1342 Veres, P., Roberts, J. M., Kuster, W. C., Reardon, J., Griffith, D. W. T., Johnson, T. J., Hosseini, S., Miller, J. W.,
1343 Cocker III, D. R., Jung, H., and Weise, D. R.: Coupling field and laboratory measurements to estimate the emission
1344 factors of identified and unidentified trace gases for prescribed fires, *Atmos. Chem. Phys.*, 13, 89-116,
1345 <https://doi.org/10.5194/acp-13-89-2013>, 2013.

1346
1347 Yuan, B., Koss, A., Warneke, C., Gilman, J. B., Lerner, B. M., Stark, H., and de Gouw, J. A.: A high-resolution time-of-
1348 flight chemical ionization mass spectrometer utilizing hydronium ions (H₃O⁺ ToF-CIMS) for measurements of volatile
1349 organic compounds in the atmosphere, *Atmos. Meas. Tech.*, 9, 2735-2752, <https://doi.org/10.5194/amt-9-2735-2016>,
1350 2016.

1351
1352 Yue, C., Ciais, P., Cadule, P., Thonicke, K., and van Leeuwen, T. T.: Modelling the role of fires in the terrestrial carbon
1353 balance by incorporating SPITFIRE into the global vegetation model ORCHIDEE – Part 2: Carbon emissions and the
1354 role of fires in the global carbon balance, *Geosci. Model Dev.*, 8, 1321-1338, <https://doi.org/10.5194/gmd-8-1321-2015>,
1355 2015.

1356
1357 Zarzana, K. J., Selimovic, V., Koss, A. R., Sekimoto, K., Coggon, M. M., Yuan, B., Dubé, W. P., Yokelson, R. J.,
1358 Warneke, C., de Gouw, J. A., Roberts, J. M., and Brown, S. S.: Primary emissions of glyoxal and methylglyoxal from
1359 laboratory measurements of open biomass burning, *Atmos. Chem. Phys.*, 18, 15451-15470, [https://doi.org/10.5194/acp-](https://doi.org/10.5194/acp-18-15451-2018)
1360 [18-15451-2018](https://doi.org/10.5194/acp-18-15451-2018), 2018.

Deleted: Xu, L., Crouse John, D., Vasquez Krystal, T., Allen, H., Wennberg Paul, O., Bourgeois, I., Brown Steven, S., Campuzano-Jost, P., Coggon Matthew, M., Crawford James, H., DiGangi Joshua, P., Diskin Glenn, S., Fried, A., Gargulinski Emily, M., Gilman Jessica, B., Gkatzelis Georgios, I., Guo, H., Hair Johnathan, W., Hall Samuel, R., Halliday Hannah, A., Hanisco Thomas, F., Hannun Reem, A., Holmes Christopher, D., Huey, L. G., Jimenez Jose, L., Lamplugh, A., Lee Young, R., Liao, J., Lindaas, J., Neuman, J. A., Nowak John, B., Peischl, J., Peterson David, A., Piel, F., Richter, D., Rickly Pamela, S., Robinson Michael, A., Rollins Andrew, W., Ryerson Thomas, B., Sekimoto, K., Selimovic, V., Shingler, T., Soja Amber, J., St. Clair Jason, M., Tanner David, J., Ullmann, K., Veres Patrick, R., Walega, J., Warneke, C., Washenfelder Rebecca, A., Weibring, P., Wisthaler, A., Wolfe Glenn, M., Womack Caroline, C., and Yokelson Robert, J.: Ozone chemistry in western U.S. wildfire plumes, *Sci. Adv.*, 7, eab13648, <https://doi.org/10.1126/sciadv.abl3648>, 2021.

1381 Zhao, X. and Wang, L.: Atmospheric Oxidation Mechanism of Furfural Initiated by Hydroxyl Radicals, The Journal of
1382 Physical Chemistry A, 121, 3247-3253, <https://doi.org/10.1021/acs.jpca.7b00506>, 2017.
1383
1384 Zheng, W., Flocke, F. M., Tyndall, G. S., Swanson, A., Orlando, J. J., Roberts, J. M., Huey, L. G., and Tanner, D. J.:
1385 Characterization of a thermal decomposition chemical ionization mass spectrometer for the measurement of peroxy acyl
1386 nitrates (PANs) in the atmosphere, Atmos. Chem. Phys., 11, 6529-6547, <https://doi.org/10.5194/acp-11-6529-2011>,
1387 2011.